

Journal of Materials Chemistry A

Accepted Manuscript



This is an *Accepted Manuscript*, which has been through the Royal Society of Chemistry peer review process and has been accepted for publication.

Accepted Manuscripts are published online shortly after acceptance, before technical editing, formatting and proof reading. Using this free service, authors can make their results available to the community, in citable form, before we publish the edited article. We will replace this *Accepted Manuscript* with the edited and formatted *Advance Article* as soon as it is available.

You can find more information about *Accepted Manuscripts* in the [Information for Authors](#).

Please note that technical editing may introduce minor changes to the text and/or graphics, which may alter content. The journal's standard [Terms & Conditions](#) and the [Ethical guidelines](#) still apply. In no event shall the Royal Society of Chemistry be held responsible for any errors or omissions in this *Accepted Manuscript* or any consequences arising from the use of any information it contains.

Self-assembled IrO₂ Nanoparticles on DNA Scaffold with Enhanced Catalytic and Oxygen Evolution Reaction (OER) Activities

S. Anantharaj[#], P. E. Karthik^{\$} and Subrata Kundu^{#*}

[#] Electrochemical Materials Science (ECMS) Division, ^{\$} Electrodeposition and Electro catalysis (EEC) Division, CSIR-Central Electrochemical Research Institute (CECRI), Karaikudi-630006, Tamilnadu, INDIA.

* To whom correspondence should be addressed, *E-mail: skundu@cecri.res.in and subrata_kundu2004@yahoo.co.in*, Fax: +91 4565-227651; Tel: +91 4565-241487.

ABSTRACT

Self-assembled IrO₂ nanoparticles (NPs) of two distinct chain-like morphologies had been successfully synthesized on DNA scaffold at room temperature by the reduction of hydrated iridium salt precursor under continuous stirring. Different morphologies of IrO₂ NPs were formed by tuning the concentration ratio of DNA to iridium salt solution. The probable growth mechanisms of the IrO₂ NPs on DNA were elaborated. The potentiality of the DNA@IrO₂ NPs were tested in two important applications, one as a catalyst for the oxidation of 2-propanol to acetone and other as an electrocatalyst for oxygen evolution reaction (OER). Catalysis study revealed that the reaction completed in a short time with higher product yield. The self-assembled, chain-like IrO₂ NPs were screened as a potential electrocatalyst for the OER study that required an overpotential of 312 mV, to produce anodic current densities of 10 mA cm⁻² (0.1 M NaOH) with turnover frequency (TOF) of 7.88 s⁻¹. This is one among the lowest oxygen overpotential reported for IrO₂ alone. The presence of phosphorous on DNA-phosphate backbone on the IrO₂ NPs surface is the key factor for the enhancement of OER activity. Though the conductivity of DNA@IrO₂ NPs modified GC becomes comparatively lower than bare GC, the synergism assisted enhancement by PO₄³⁻ from DNA in the overall OER activity makes it worthier still. The overall processes is simple, less time consuming, reproducible, occur at room temperature and can be extended for the synthesis of other important nano-catalysts at a short time scale for their applications in different interdisciplinary fields like organic catalysis and in electrocatalysis.

Introduction

In recent years, controlled syntheses of nanomaterials with specific size and morphology have found huge attention in all the field of science and technology. Nanomaterials exhibit unique physico-chemical properties due to their ultra-small size and large surface to volume ratio. Nanomaterials can be applied in different emerging fields such as nanoelectronics,¹ catalysis,² sensing,³ biology,⁴ solar cell,⁵ supercapacitor⁶ and in surface enhanced Raman spectroscopy(SERS) studies.⁷The controlled synthesis of nanomaterials such as nanotubes, nanorods, nanowires and others are essential due to their wide range of applications.⁸⁻⁹ Studies on the synthesis and applications of metal and semiconductor nanomaterials with either 1D shape or assembly are rich compared to other systems like metal oxide and mixed metal oxide nanomaterials. Hence, it is important to figure out an easy and facile route for the synthesis of size and shape controlled 1-D metal oxide nanostructures within a short time scale for which wet chemical routes via bottom up approach are more advantageous compared to the physical routes. Among the different transition metal oxides used as catalysts, the iridium oxide (IrO_2) nanomaterials have attracted great attention due to their remarkable use in oxygen reduction reaction (ORR),¹⁰ oxygen evolution reaction (OER)¹¹ and methanol fuel cell reactions.¹² Despite the high cost and low terrestrial abundance of iridium, the iridium oxide based nanoparticles (NPs) with high surface area to mass ratio have been widely studied similar to that of Pt NP, for fuel cell applications.¹³ Moreover, IrO_2 is the state-of-the-art catalyst in OER.¹⁴Nowadays, different types of bio-molecules have been being utilized for the syntheses and self-assembling of nanomaterials. Among them, different bio-molecules such as amino acids, peptides and proteins, the deoxyribonucleic acids (DNA) have been of much interest as a potential template to build various inorganic nanostructures. DNA is extensively used as a template which renders the chain-like morphology and acting as a stabilizing agent for the synthesized materials. Different metal, metal oxide and semiconductor nanomaterials like Au,¹⁵ Ag,¹⁶ Pt,¹⁷ Pd,¹⁸ Os,¹⁹ Cu,²⁰ Fe_2O_3 ,²¹ ZnO,⁵ TiO_2 ⁶ and CdS¹ were self-assembled on DNA template. Nonetheless, there is no report for the self-assembly of IrO_2 NPs on DNA scaffold. IrO_2 nanomaterials synthesis has been done in many methods.¹⁴ Malonate and succinate stabilized IrO_2 nanomaterials.^{22,23} The synthesis of uncapped IrO_2 NPs through alkaline route resulted in different color solution from pale blue to deep blue. Meanwhile, in acidic pH (below 3), they got precipitated. Although they

are stable when formed via alkaline hydrolysis, the precipitation occurred at neutral pH.²⁴ Beyond these, there is another report for the syntheses of IrO₂ nanomaterials for other applications.²⁵ However, it is important to state that most of the above reports took long reaction time, multiple steps, utilized toxic chemicals, electrochemical assistance or the resultant particles lacked in monodispersity. Hence, it is highly desired to figure out an easy and quick method for the controlled generation of IrO₂ nanomaterials which can be used as potential catalyst in OER by catalyzing the following reactions in acidic and basic medium respectively.¹⁴



Although many material like, metal oxides,^{26,27} mixed metal oxides,²⁸ complexes of transition metal ions,²⁹ phosphometallates and metal phosphates,^{30,31} polyoxometallates,^{32,33} perovskites,³⁴ metal oxynitrides,³⁵ and sulphur based semiconductors³⁶ are reported for OER, IrO₂ nanomaterials are known for their best activities in OER. Among the several reports on the OER activity by IrO₂, significant reports are as follows, Murray and co-workers studied the electrocatalytic activity of hydrated IrO₂ film in a wide range of pH.³⁷ Karthik et al. reported the electroless deposition of IrO₂ NPs on an anodized Au surface and studied their electrocatalytic activity towards OER studies.³⁸ Unfortunately, there was a report by Strasser et al. which claimed that the bulk IrO₂ showed better catalytic activity towards OER than the IrO₂ at nano level.³⁹ According to their claim the change in electronic effect while decreasing the dimension of IrO₂ from bulk to nano decreased the OER kinetics, especially in the case of Ir, Pt and Pd. Nevertheless, after that many had reported that nano IrO₂ as a single particle,⁴⁰ colloidal,⁴¹ electrogenerated dissolved particles,⁴² colloidal IrO₂ conjugated with a complex,⁴³ self-assembled IrO₂ in ITO plates,⁴⁴ 3-D macroporous IrO₂,⁴⁵ ligand and photosensitizer controlled IrO₂,²⁴ IrO_x core-shells,⁴⁶ electrolessly deposited IrO₂ particles on anodized gold surface³⁸ and biologically templated IrO₂ particles are found to be highly active towards water oxidation.⁴⁷ Till now, the lowest overpotential for IrO₂ electrocatalyst was reported by Jaromillo et al. which is 10 mA.cm⁻² at 325 mV.⁴⁸ On the other hand, Shao-Horn et al. reported the orientation dependent enhanced OER activity of IrO₂ nanostructures⁴⁹ Interestingly, phosphate groups and phosphorous compounds are reported to be highly active and showing lower oxygen overpotential than others. A very important report by Nocera et al. says that in-situ generated

cobalt phosphates from a neutral phosphate buffer solution of Co^{2+} ions which showed higher catalytic activities than cobalt oxides. This is mainly due to the synergism between the higher affinity of phosphate groups toward water and electrocatalytic property of Co^{2+} ions.⁵⁰ Similarly, Bond et al. studied the OER in presence of phytic acid which is an organic acid that contains six phosphoric acid residues connected to a cyclohexane base ring and found similar synergism.⁵¹ Very recently, Stern et al. reported the OER activity of Ni_2P which on anodizing during water oxidation forms NiO_x that contains considerable amount of phosphate ligands shell with Ni_2P . They achieved the lowest overpotential ever reported for OER in alkaline medium of 290 mV to generate 10 mA cm^{-2} of current densities due to the synergism between phosphate group and NiO_x catalyst.⁵² Besides, OER catalyts are significant nowadays, as they are essential in metal-air batteries. Reports of Li et al. are the examples where NiCoO_4 and IrO_2 have been extensively studied for Li-air batteries as OER nanocatalyts.^{53,54} Apart from the electrocatalysis, transition metal oxides and their complexes are the most frequently used catalyts in many organic reactions, including the simple ones to asymmetric synthesis. Functionalization of C-C bonds,⁵⁵ C-C bond formations,⁵⁶ coupling of C-C multiple bonds,⁵⁷ asymmetric epoxidation and asymmetric dihydroxylation⁵⁸ are the familiar reactions which employ transition metal/metal oxides/metal complexes. Recently, Punniyamurthy et al. highlighted in his review articles about the recent development of transition metals, metal oxides and their complexes as catalyts and their uses in organic reactions.⁵⁹ Oxidation of alcohols is the relatively most appropriate and fundamental organic reaction for checking the catalytic activity of a transition metal oxide. Transition metal oxides play colossal roles as catalyts as well as reagents in organic chemistry. Alcohols are oxidized easily in the presence of a transition metal oxide whose electron affinity is much increased in the presence of an acid.⁶⁰

In this present report, for the first time, we highlighted the syntheses of uniform, self-assembled IrO_2 NPs on DNA scaffold within a short reaction time at RT. With a large literature support given above, we applied our IrO_2 NPson DNA scaffold as a potential catalyts for the oxidation of 2-propanol for the very first time in acidic conditions. The detailed literature survey revealed that an electrocatalyts with a phosphate group either coordinated with it or in the vicinity will increase its electrocatalytic activity in OER. As we had successfully assembled IrO_2 NPs onto a bio-template which is having enormous phosphate functional groups in its backbone, we applied our materials for OER in alkaline condition. In 2-propanol oxidation, 83% yield was

achieved with 100% electivity within 3 h. The OER study revealed that the self-assembled, chain-like IrO₂ NPs had shown enhanced activity and required an overpotential of 312 mV, to generate anodic current densities of 10 mA cm⁻² (0.1 M NaOH) with TOF of 7.88 s⁻¹. This is one among the lowest oxygen overpotential ever reported on IrO₂ surface alone. Moreover, the present synthesis route is extremely less time consuming, simple, and environmental friendly.

Experimental Section

Reagents and Instruments.

Double-stranded DNA (Herrings Testes) with an average molecular weight of ~ 50K bp (base pair), sodium borohydride (NaBH₄) and hydrated iridium trichloride salt (IrCl₃ . xH₂O) was purchased from Sigma-Aldrich. Concentrated sulphuric acid was purchased from RANKEM Pvt. Ltd. India and 2-propanol was purchased from SRL, India. The electrochemical analyzer BAS 100B, Hg/HgO reference electrode, Pt counter electrode and GC working electrode of 6 mm diameter were purchased from Sigma-Aldrich. Mill-Q water (18 MΩ.cm⁻²) was used for the entire synthesis process. The synthesized DNA@IrO₂ NPs were characterized using several spectroscopic and microscopic techniques and the detailed specifications of the different analytical instruments used are given in online supporting information (SI) section.

Wet Chemical Synthesis of Self-Assembled, Chain-like IrO₂ NPs on DNA Scaffold.

Self-assembled, chain-like IrO₂ NPs had been synthesized by the reduction of iridium salt solution with NaBH₄ in the presence of DNA at RT. In a typical reaction, 1 mL of the stock DNA solution was mixed with 2 mL of IrCl₃.xH₂O solution and stirred well for 5 min. The solution color was pale green at the beginning due to hydrated iridium salt. Then freshly prepared 1 mL of ice-cold NaBH₄ solution (0.1 M) was added with constant stirring. The color of the solution changed from pale-green to brown as soon as borohydride was added. Even then stirring was continued to another 5 min where the solution color was found to be changing from brown to light bluish again. The bluish color indicated the formation of IrO₂ NPs in the solution. The bluish color remained stable for more than 4 months in ambient condition both under dark and in light. By adapting the similar protocol, another set was also prepared by varying the DNA concentration. With increasing the concentration of DNA, the time taken for the completion of

the reaction was also found to be increasing. A comprehensive detail on final concentration of all the reagents, reaction time, solution color, particle size and morphology are elaborated in Table 1. The formation of the self-assembled IrO₂NPs on DNA scaffold is depicted in Scheme S1 in online SI section. The preparation of samples for various instrumental characterizations is elaborated in-detail in the online supporting information (SI) section.

Liquid Phase Oxidation of 2-propanol to Acetone using Self-Assembled DNA@IrO₂ NPs.

The catalytic activity of both the DNA@IrO₂ NPs with two different morphologies were tested for the liquid phase oxidation of 2-propanol. In two different double necked round bottom (Rb) flask, 1.25 mL of 2-propanol was mixed with 1.25 mL solution of DNA@IrO₂ NPs of average individual particle size of 3.5 ± 0.3 nm in one and of 5.5 ± 0.3 nm in another one along with 0.05 mL of conc. sulphuric acid in both. One neck of the Rb flask was connected to a condenser which is inserted into another Rb flask kept in ice cold water. The whole content was heated and stirred simultaneously using a magnetic stirrer. Another neck of the Rb flask was closed to ensure that the product formed was not lost. The temperature was slowly raised up to 60°C. Beyond 56 °C, the condensation of liquid product in the Rb flask kept in ice cold water was observed. The reaction was continued for a slot of 3 h. Initially, the color of the reaction mixture was violet which is characteristic of IrO₂ NPs. The violet color slowly turned pale green at the end of the reaction that implied that the IrO₂ was converted into its lower oxides in which iridium was in an oxidation state less than 4. One of the neck of Rb flask was opened and the catalyst was exposed to atmospheric oxygen which turned the catalyst immediately to violet again indicated that IrO₂ NPs were formed again. Then the reaction vessel was shut and the reaction was continued. But, No more condensation of product was observed. The condensed product was further confirmed with UV-Vis, FT-IR and ¹H NMR analyses as discussed in the ‘catalysis part’ under results and discussion section.

Electrode Fabrication and Oxygen Evolution Reaction (OER) studies.

In brief, for the whole electrocatalytic study, a glassy carbon (GC) electrode was used as the working electrode with necessary surface modifications with Pt counter electrode and Hg/HgO reference electrode. In heterogeneous OER, the surface of the GC electrode was modified by drop casting 6 μL of the solution of DNA@IrO₂ NPs on the GC surface and dried in

room temperature. The surface modified GC electrode was inserted into an electrolytic cell which contained a Pt counter electrode and a Hg/HgO reference electrode. About 20 mL of 0.1 M sodium hydroxide solution was taken as electrolyte. Since we found that DNA has good adhesion property on GC surface, we did not use any additional specific binder to our material. The whole electrochemical set up was connected to an electrochemical workstation and done all the electrochemical studies that are essential.

Results and Discussions

UV-Visible Study.

The electronic spectra of the different solution mixture for the formation IrO₂ NPs are shown in Figure 1. In Figure 1A, curve a is the absorption spectrum of IrCl₃.xH₂O salt solution which has no specific absorption band but a broad peak near 300 nm might be due to the hydration of Ir³⁺ ions and the formation of [Ir(OH)₆]²⁻ complex.^{61,62} Curve b shows the absorption band of aqueous DNA solution which has a well-known absorption band at 257nm due to absorption of aromatic base pairs. Curve c, Figure 1A shows the absorption band of the aqueous solution mixture of iridium chloride salt solution with DNA where we can see that the DNA peak is shifted a bit towards the higher wavelength side at 260 nm and a new broad hump near 345-400 nm with low intensity was observed which indicated the adsorption of Ir³⁺ ions on DNA molecules. After mixing NaBH₄ solution under stirring condition, the solution color changed from green to brown to light blue which indicated the formation of IrO₂NPs in the solution. By changing the DNA concentration and keeping other parameters intact the reaction took different time to complete. Curve d, Figure 1A shows the absorption band of IrO₂NPs in which, a DNA peak at 260 nm, an absorption hump at ~ 312 nm and anew peak with low intensity at 572 nm appeared that indicates the conversion of [Ir(OH)₆]²⁻ to IrO₂ NPs. Curve e also shows the absorption bands of IrO₂ NPs with different DNA concentration as given in Table 1. Here DNA peak observed at 260 nm and absorption hump was appeared at ~ 318 nm. Figure 1B shows the enlarged absorption band of the IrO₂NP for two different sets where curve a shows an absorption band 572 nm and curves b show an absorption bands at 582nm. The successive shifting of λ_{\max} value to higher wavelength region indicated the formation of bigger/larger size particles which is a common phenomenon in nanoscale synthesis of materials.⁶³ The inset of Figure 1A shows the two differently colored IrO₂ NPs solution for two different morphology

(light blue color for small size and deep blue color for larger size). The absorption bands observed in present study are matching properly with IrO₂ NPs reported by Mallouk and others.^{27, 61, 64}

Transmission Electron Microscopy (TEM) Analysis.

Transmission electron microscopic (TEM) micrographs of the self-assembled, chain-like IrO₂ NPs on DNA scaffold are shown in Figure 2. The low and high magnified TEM micrograph of the self-assembled IrO₂ NPs having chain-like morphology with smaller average particle size are shown in Figure 2, A-C respectively which gave the absorption curve a in Figure 1B. From the low magnified micrograph, it is clear that the IrO₂ NPs are self-assembled and aggregates of DNA chains and formed the chain-like structure. The average size of the particles obtained from the particle size histogram which is given as an inset image in figure 2C is $\sim 3.5 \pm 0.3$ nm. Figure 2C is the high magnified TEM micrograph of the same samples where the individual particles on the DNA chains are clearly visible. The average length of the chains assembled by IrO₂ NPs is $\sim 1-1.5$ μm . From these micrographs, it is also observed that few DNA chains are self-assembled or cross-linked together to generate the small size chain-like structure and the diameter of the chains vary from 35 ± 2 nm. Figure 2D is the HR-TEM micrographs of the first set where very small IrO₂ particles with fine crystal fringes are observed. The lattice spacing between two individual planes are calculated ~ 0.2246 nm that corresponds to (111) plane. Apart from this, there are couple of others phases also visible which are assigned accordingly in the HR-TEM micrograph (Figure 2D). Figure 2E is the corresponding selected area electron diffraction (SAED) pattern which indicates the IrO₂ particles are crystalline in nature and forming ring patterns due to their size. However, the rings are assigned accordingly to their corresponding diffraction planes that found good agreement with the XRD analysis carried out earlier and to the JCPDS card number 43-1019. Although we did not analyze our samples beyond 90° in XRD analysis, The larger ring is observed in SAED pattern that originates from (412) plane which corresponds to the 2θ value of 118.28° in XRD analyses. Similarly, the low and high magnified TEM micrograph of self-assembled IrO₂ NPs having chain-like morphology on DNA scaffold with comparatively larger average particle size, are shown in Figure 2, F-H (corresponds to curve b in Figure 1B). From the low magnified micrographs in Figure 2F and 2H, it is seen that relatively larger size IrO₂ NPs are self-assembled and grown on the DNA chain to generate the

chain-like morphology. From the micrograph, it is seen that the diameter of the chains are not fully uniform which might be due to uneven aggregation of DNA during synthesis. The average size of the individual IrO₂ NPs on DNA are $\sim 5.5 \pm 0.3$ nm whereas the average diameter of the chains are $\sim 26 \pm 2$ nm. In certain cases, few chains are cross-linked each other. The nominal length of the chains decorated by IrO₂ NPs is $\sim 1-2$ μ m. The inset of Figure 2F shows the corresponding particle size distribution histogram. Figure 2I is the HR-TEM micrograph of the second set where relatively larger IrO₂ particles with fine crystal fringes are observed. The lattice spacing between two individual planes are calculated ~ 0.2245 nm that corresponds to (111) plane. Here also, others phases are visible that are assigned respective to their diffraction planes. We did not observe any separate spots in the SAED (Figure 2J) pattern this might be due to very small size of the individual particles which do not diffract the electron beam. However, the obtained rings are assigned with their corresponding diffraction planes as shown in Figure 2J. From TEM, HR-TEM and SAED analyses, it is confirmed that mono-dispersed IrO₂ NPs (of different sizes) are formed by changing the reagents concentrations, which was directed to uniformly grew over the DNA chains, and gets self-assembled together to generate the chain-like morphologies.

EDS Analysis.

Energy dispersive X ray spectroscopic analysis was used to identify the elements present in our synthesized nanomaterials solution. Figure S1 (online SI section) shows the EDS spectrum which contains different peaks for Ir, Cl, O, Ca, Si, P and Na. The Ca and Si peak came from the glass substrate used to deposit IrO₂ NPs during the EDS sample preparation. The Cl peak came from the iridium chloride salt and the O peak came from the IrO₂ NP and from the DNA. The P peak came from the DNA which is used during the synthesis of IrO₂ NPs. The EDS analysis clearly confirms and supports the formation of IrO₂ NPs on DNA scaffold as witnessed by TEM analysis.

X-ray Diffraction (XRD) Analysis.

X-ray diffraction (XRD) pattern of the DNA@IrO₂ is shown in Figure 3 where line a and line b correspond to XRD pattern of small and large size IrO₂ particles respectively. Different diffraction peaks were observed at 2 θ values 28.4°, 34.6°, 40.0°, 40.2°, 44.7°, 54.02°, 58.8°, 76.8°, 65.7°, 76.2° and 83.6° were corresponding to (110), (101), (200), (111), (210), (211),

(002), (221), (212) and (321) planes respectively. All these peaks are confirming the formation of IrO₂ NPs having space group P4₂/mmn with respective JCPDS card number of 43-1019.^{14,65,66} The XRD analysis was performed in the 2θ range of 10-90°. Few peaks with negligible intensities observed between 45° to 50° may be due to some of the iridium hydroxide formed due to the hydration of synthesized IrO₂ NPs on DNA. The XRD pattern for both samples clearly indicates that change in DNA concentration does not affect the crystallization and growth of IrO₂ particles on DNA scaffolds. From Figure 3, it is clear that regardless of DNA concentration, the iridium oxide nuclei had grown preferentially in (111) plane compared to other facets. The same is clearly evidenced from SAED (Figures 2E and 2J) and HR-TEM analyses.

X-ray Photoelectron Spectroscopy (XPS) Analysis.

The overall XPS survey spectrum is given in Figure 4A and Figures 5, B-G are the high resolution spectra of Ir 4d, Ir 4f, C 1s, P 2p, O 1s and N 1s peaks respectively. The survey spectrum has different peaks for Na 1s (at 1071 eV), O 1s (at 532.3 eV),⁶⁷ Ir 4d (at 313.5 eV and 297.2 eV),⁶⁸ N 1s (at 400.9 eV),⁶⁹ C 1s (at 284.6 eV),⁷⁰ P 2p (at 132.9 eV),⁷¹ Ir 4f (at 62.1 eV and 64.8 eV)^{68,72} and P 3s (at 18.5 eV)⁷³ respectively at their expected binding energy values. Figure 4B is the high resolution spectra of Ir 4d peaks which are characterized by a doublet arises due to spin orbit coupling (4d_{3/2} and 4d_{5/2}). The peak positions of Ir 4d_{3/2} and 4d_{5/2} are at 313.5 eV and 297.2 eV binding energies respectively as expected.⁶⁸ A small hump near Ir 4d_{5/2} at 302.5 eV is attributed to the satellite peak of the same state. Figure 4C is the high resolution spectra of Ir 4f peak with a doublet at the region where the Ir 4f peaks are supposed to be appeared for IrO₂.^{68,72,74-76} The peak was deconvoluted and fitted accordingly where we can see two deconvoluted peaks at 62.1 eV and 64.8 eV for Ir 4f_{7/2} and Ir 4f_{5/2} states respectively. The binding energy values of both Ir 4d and Ir 4f states clearly confirmed the presence of tetravalent Ir⁴⁺ ions in our synthesized material which in turn confirmed the formation of IrO₂.^{68,72,74-76} The high resolution XPS peaks of C 1s is shown in Figure 4D. Appearance of various peaks at the binding energy values of 284.6 eV, 285.7 eV, 287.7 eV and of 290.2 eV are confirming the presence of various carbon functionality such as C=C, C=O, C=NH, C-O-R and C(O)-NH- that are originated from the DNA and also in agreement with previous reports.^{70,77-79} Figure 4E is the high resolution spectra of P 2p with a doublet due to spin-orbit coupling. Both P 2p_{3/2} and P 2p_{1/2} were observed at 132.9 eV and 134.5 eV respectively that denote the presence of P⁵⁺ ions.⁷¹

Figure F is the high resolution of O 1s with two peaks at 532.5 eV and 534.4 eV as expected.^{67,80-82} The high resolution spectra of N 1s is given as Figure 4G where the characteristic peak at 400.9 eV corresponds to the trivalent N atom with sp^2 hybridization. The detailed XPS analyses confirmed that both DNA and IrO₂ NPs are together as witnessed by TEM and the oxidation state of iridium ion is +4 which confirmed the formation of IrO₂ NPs. Similarly, the XPS analysis for smaller size IrO₂ particles had also been carried out and found similar results (not shown here) indicating that although the morphology is different but the chemical nature remains the same.

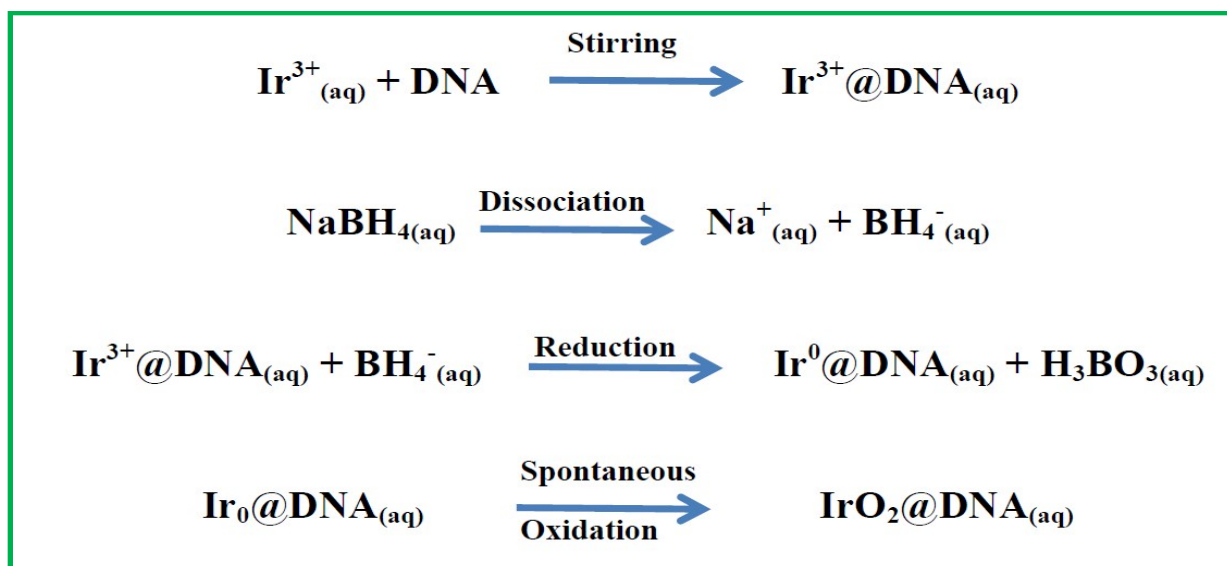
Fourier Transform Infrared (FT-IR) Spectroscopic Analysis.

The Fourier transform infrared (FT-IR) spectrum of bare DNA and DNA encapsulated IrO₂ nanomaterials are shown in Figure 5. In the FT-IR spectrum curve 'a' is denoted for DNA alone and curve 'b' is for DNA@IrO₂ NPs. The detailed FT-IR analyses from both the spectra 'a' and 'b' signified that the DNA molecules are either present inside the IrO₂ or on the surface of the IrO₂ NPs which also revealed that there were interactions between DNA and IrO₂ NPs. From curve a (of only DNA), some intense bands in lower wavenumber region at 560 cm⁻¹, 812 cm⁻¹ and 1105-1220 cm⁻¹ are seen due to the stretching vibration of phosphate group in DNA and from the glass substrate. In case of DNA bound IrO₂, the positions of some peaks were shifted or completely disappeared and some new peaks were observed as seen in curve b. The peak observed at 1273 cm⁻¹ in the case of only DNA is largely shifted to 1229 cm⁻¹ in case of DNA bound IrO₂ NPs. Similarly, two small sharp peaks at 1511 cm⁻¹ and 1678 cm⁻¹ due to carbonyl and C-O-X groups for DNA were also shifted which indicates interaction of IrO₂ with the DNA molecule. Vibrations of C-H bonds of methylene group was poorly observed in case of DNA@IrO₂ NPs. For only DNA the peaks appeared at 3606 cm⁻¹ and 3738 cm⁻¹ were shifted and appeared as a broad peak at 3708 cm⁻¹ for DNA@IrO₂ NPs. For DNA bound IrO₂ samples a strong peak appeared at 485 cm⁻¹ was due to the characteristic absorption of Ir-O-Ir bond which is absent for only DNA which indicates the attachment of IrO₂ with DNA. As there was no report for FT-IR band of IrO₂, we compared our results with the similar type of FT-IR spectra shown by DNA templated MnO₂ which also showed a band at lower wavenumber region which was assigned to Mn-O-Mn stretching.⁸³ The FT-IR bands of DNA experimentally observed in our study and the previously reported FT-IR bands⁸⁴ were elaborated in Table S1 (in SI section). The

FT-IR analysis for small size DNA@IrO₂ NPs was also carried out and found similar transmittance features (not shown here) which suggest similar binding nature of both IrO₂ particles on DNA scaffolds.

Mechanism for the Formation of Self-Assembled IrO₂ NPs on DNA Scaffold.

Self-assembled IrO₂ NPs on DNA scaffold having chain-like morphology were synthesized by the reaction of IrCl₃.xH₂O salt with NaBH₄ in the presence of DNA under continuous stirring at RT. The specific concentrations of different reagents, size, and morphologies of two different sets are elaborated in Table 1. The specific role of the presence of different reagents was elaborated by couple of control experiments. Initially, the reaction was carried out without DNA keeping reaction time and other reaction conditions as the same as did earlier and observed IrO₂ particles were formed but precipitated immediately after the addition of borohydride. The second one was carried out in absence of borohydride and observed no reaction. These confirmed that the presences of all the reagents were extremely important. The color of the aqueous Ir³⁺ solution was greenish due to ligand to metal charge transfer (LMCT).⁸⁵ The chemical reaction took place between Ir³⁺ salt and NaBH₄ is given below.



Hence, it is clear that the Ir³⁺ ions are reduced by the borohydride to form Ir⁰ metal nuclei on the DNA chain which then grew along the DNA chain. As the borohydride added were

consumed, the spontaneous oxidation Ir^0 to IrO_2 was the predominant process which ultimately generated the self-assembled IrO_2 NPs as a chain-like morphology. FT-IR analyses revealed that IrO_2 NPs are bound with the DNA molecules mainly via the phosphate group, hydroxyl group of deoxyribose sugar entities and aromatic bases present in DNA backbone. The Ir^{3+} ions were attached to the DNA molecules due to electrostatic interactions as confirmed by the shift of the respective UV-Vis absorption spectrum of the mixture of DNA and Ir^{3+} aqueous salt solutions (curve c, Figure 1A). These IrO_2 particles generated by the re-oxidation of Ir^0 were witnessed primarily from the color change observed from brown to violet. We observed that when DNA concentration was low, the IrO_2 particles were formed within 5 min but when the DNA concentration was increased gradually, it took more time to form IrO_2 NPs. Hence, we believed that at lower DNA concentration, a part of Ir^{3+} ions were attached to DNA first with some free Ir^{3+} ions in the solution which were not attached to DNA. As BH_4^- was added, the free Ir^{3+} ions were immediately reduced to form Ir^0 which acted as a catalyst for the reduction of remaining Ir^{3+} ions attached with the DNA. Finally, within a short time all the Ir^{3+} ions were reduced and turned into brown Ir^0 NPs initially and then spontaneously formed a light blue color solution that indicated the successful formation of IrO_2 NPs. At higher DNA concentration, all the Ir^{3+} ions were adsorbed onto DNA and successive reductions took longer period to generate the IrO_2 NPs. At low DNA concentration, the individual particle size is large and chain diameter is small. On the other hand, at higher DNA concentration, individual particles are comparatively smaller but chain diameter is larger. We believed that at low DNA concentration, due to unrestricted growth as there was limited number of dispersed DNA molecules nearby large particles were formed. Besides, the corresponding chain diameter was smaller at low DNA concentration. This is because, at low DNA concentration, the probability of self-agglomeration among them is less which results smaller chain diameter. While at higher DNA concentrations, restricted growth due to the availability of more number of DNA molecules over the IrO_2 particle results in small particles. However, the corresponding chain diameter is larger due to availability of more number of DNA molecules in solution. We observed similar outcomes in our earlier works for TiO_2 and Os nanocrystals.^{6,19}

Catalytic Oxidation of 2-propanol to Acetone using DNA@ IrO_2 NP as a Catalyst.

We investigated the catalytic activity of both the synthesized IrO₂NPs taking 2-propanol oxidation. If a catalyst is able to convert a secondary alcohol into its corresponding carbonyl compound that will convert all other alcohols that are comparatively easy to oxidize. There is a bunch of reports on the oxidation 2-propanol to acetone. Some of them are dealing with its mechanistic aspects whereas some others are dealing with the kinetics at different reaction conditions.⁸⁵⁻⁸⁹ To the best of our knowledge, there is no report on IrO₂NPs in any form as a catalyst for the oxidation of 2-propanol. To check the actual influence of IrO₂ in the oxidation of 2-propanol, two different control experiments were carried out as follows. The first was done without IrO₂ NPs but keeping all other remaining constituents of the original reaction mixture the same. The second was carried out with addition of 1 mL of the same DNA solution keeping other reaction conditions the same but without any IrO₂ NPs as catalyst. None of them were able to effect the oxidation of 2-propanol and it was concluded that the overall oxidation of 2-propanol was effected solely by the catalytic activity of IrO₂. The product was characterized using UV-Vis, FT-IR and FT-NMR studies as discussed below. The chemical reaction occurred is depicted below.

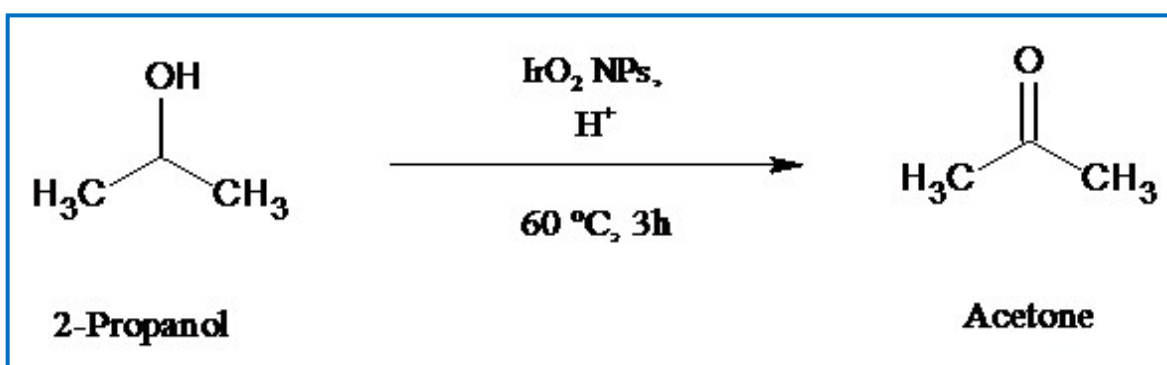


Figure 6A is the corresponding UV-Vis spectra of 2-propanol, reaction mixture before and after the reaction and the product acetone separately. Curve a is the absorption spectrum of 2-propanol which almost shows a flat line. It was quite expected, as n-σ* is the only possible transition in 2-propanol which will occur in far UV region. Curve b is the absorption spectra of reaction mixture before the reaction which shows no specific peak. Curve c is the absorption spectrum of the reaction mixture just after the reaction which has a small hump near to 280nm may be due to the residual acetone existing in the mixture after the distillation and condensation process. Curve d shows a strong absorption maximum at 278.6nm which is the characteristic

peak of acetone due to $n-\pi^*$ transition. Figure 6B shows the FT-IR spectra of both 2-propanol and the product acetone. Curve a denotes the FT-IR spectrum of 2-propanol which has peaks at 3378 cm^{-1} , 2965 cm^{-1} , 2876 cm^{-1} , 1651 cm^{-1} , 1467 cm^{-1} , 1337 cm^{-1} , 1296 cm^{-1} , 1126 cm^{-1} , 942 cm^{-1} and 817 cm^{-1} respectively. All peaks are perfectly matching with the observed spectrum of 2-propanol. The peak at 3378 cm^{-1} is due to $-\text{O}-\text{H}$ stretching vibration. Peaks at 2965 cm^{-1} and 2876 cm^{-1} are due to the asymmetric and symmetric stretching vibrations of $-\text{C}-\text{H}$ bonds. Peaks at 1651 cm^{-1} and 1567 cm^{-1} are observed due to $\text{C}-\text{C}$ stretching vibrations. Peaks at 1296 cm^{-1} and 1337 cm^{-1} are due to deformations of $-\text{C}-\text{H}$ bonds. A peak at 1126 cm^{-1} is assigned to the stretching vibration of $-\text{C}-\text{O}$ bond in 2-propanol. Figure 6B, curve b is the FT-IR spectrum of acetone obtained by the oxidation of 2-propanol which has peaks at 3460 cm^{-1} , 2965 cm^{-1} , 1739 cm^{-1} , 1636 cm^{-1} , 1429 cm^{-1} , 1356 cm^{-1} , 1216 cm^{-1} , 1112 cm^{-1} and the fingerprint region. The peak at 1739 cm^{-1} is a lone evidence which confirms that 2-propanol is oxidized to acetone whereas this peak is not observed in the FT-IR spectral profile of 2-propanol. Figure 6C, curve a is the NMR spectrum of 2-propanol in D_2O where four peaks respectively at 1.0 ppm, 2.1 ppm, 3.8 ppm and 4.6 ppm were seen. The corresponding peaks at a specified chemical shift values at 1.0 ppm for six methyl protons, 2.1 ppm for a single hydroxyl proton and 3.8 ppm for a single proton in the tertiary carbon of 2-propanol respectively. The peak at 4.6 ppm is due to the solvent D_2O which exchanges proton with 2-propanol and residual water in it. Figure 6C, curve b corresponds to the NMR spectra of acetone. A single peak at 2.3 ppm is due to the six unique protons present in an acetone molecule and the peak at 4.6 ppm is again due to the solvent D_2O . From these observations, it is confirmed that the conversion of 2-propanol to acetone occurred successfully catalyzed by IrO_2 NPs. The recyclability of the catalyst found more than five times and it was found effective up to three cycles beyond which effectiveness in converting 2-propanol to acetone gradually fell down regularly. This is the quite expected result of every homogeneous catalysis reaction. The yield of the final product was $\sim 83\%$. Besides the fact of economical un-affordability, the advantages of this method can be summarized as; this is non-toxic and reproducible and eases of conduction and the applicability in some areas where the toxic oxyanions like dichromate and permanganate cannot be used. Moreover, in catalysis, as IrO_2 is anchored on DNA, the probability of leaching becomes smaller since DNA is much bulkier than the reactant and product of the catalysis study, at $60\text{ }^\circ\text{C}$ DNA won't be volatilized. In near future, this work

will be extended to other organic reactions and an intense effort will be made to minimize the iridium content thereby minimizing the cost of the total catalyst preparation.

Electrocatalytic Activity towards the Oxygen Evolution Reaction (OER) by Self-assembled IrO₂ NPs on DNA Scaffolds.

Figure 7A is the respective linear sweep voltammogram (LSV) run at a scan rate of 0.01 V/sec where line a is corresponding to LSV with *i*R drop correction and line b is of without correction. The benchmarking anodic current density of 10 mA.cm² is observed at 1542 mV. Resistance of the system was measured by carrying out the electro impedance (EI) spectroscopy for bare and DNA@IrO₂ NPs modified, DNA modified and IrO₂ modified GC electrodes separately which are given as Figures 7, B-D. From these EI spectra, the solution resistance of these systems was calculated for these modified electrodes from their respective EI spectra and the resultant LSVs of all these modified GC were corrected accordingly. From these EI spectra we can notice that in all the three cases bare GC had low resistance than DNA modified, IrO₂ modified or DNA@IrO₂ modified GC electrodes. Moreover, from these EI spectra, it is also evident that DNA modified GC had relatively low resistance compared to other two modified electrodes. This is attributed to the conducting nature of DNA. Although, it is important to note here that the presence of PO₄³⁻ group in DNA is most important parameter for the synergistic enhancement in the overall OER activity. The kinetics of the same reaction was further studied by plotting Tafel curve which is given as Figure 8A. It can be seen from the Figure 8A, at higher and lower over potential regions the order of Tafel slopes was 90 mV/dec and 32 mV/dec. As it is known that, for a one electron transfer reaction where $\alpha = 0.5$ Tafel slope should be 120 mV/dec. Water oxidation could be a 1 to 4 electron transfer depending on the condition and potential applied. Hence, the approximate rate determining step and the number of electron transfer at these regions can be predicted on the basis of Tafel slope as per literature.⁹⁰⁻⁹² As we observed 32 mV/dec at lower overpotential, four electron transfer process would be predominant. Similarly, at higher overpotential region the order of observed Tafel slope is 90 mV/dec which advocates that two electron process would be predominant (details in SI section).⁹⁰⁻⁹² Predicting number electron transfer in a reaction based on Tafel slope had been intensively studied by Shinagawa et al. for OER, ORR, HER, HOR and other similar aqueous electrocatalytic reactions where O₂ and H₂ are involved by constructing kinetic models.⁹² They had concluded that the

prediction of number electron transfer occurred can be made using Tafel slopes both at lower and higher overpotential region if $\alpha \approx 0.5$. To figure out the stability of our catalyst modified GC electrode and to know the negative effect of catalyst leaching on prolonged reaction, a chronoamperometric study was carried out using the same cell and electrodes. The respective current versus time plot is given as Figure 8B. From the Figure 8B, it was well understood that our catalyst was able to survive more than 12 h continuously without any loss in the current density. To ensure this, after the chronoamperometry analysis, an LSV was carried out under the same experimental conditions and found very small and negligible shift in the overpotential which certainly tells us that there is no or highly negligible amount of leaching even after 12 h and the corresponding figure is given as Figure S2 in online SI section. Although the constant potential electrolysis result revealed that DNA@IrO₂ NPs modified GC is stable for more than 12 h. We have conducted a cycling test on the same DNA@IrO₂ NPs modified GC by running 200 consecutive cycles of CV at a scan rate of 10 mV/s between 0 to 1 V vs Hg/HgO reference electrode. The obtained CV at 1st, 50th, 100th, 150th and 200th cycle are given together as Figure 9. From Figure 9, it was seen that at catalytic turnover condition (10 mA/cm²), the drop in potential upon prolonged cycling is not more than 25 mV. The observed negligible drop while sweeping the potential between 0 to 1 V in alkaline medium might be due to leaching and passivation of the catalyst in GC surface. Beyond the catalytic turnover condition, the drop in potential is increased to a notable extent. Moreover, to find out the role of each component in our electrocatalytic study, a set of controlled experiments were carried out as follows. An LSV was run at the same potential window under the same experimental conditions but with a GC electrode modified only with the same quantity of DNA stock solution as that of the catalyst used for the synthesis of the material. Similarly, another LSV was run at the identical conditions but this time with a GC electrode modified by IrO₂ particles prepared using the same wet chemical protocol but without the DNA scaffolds. Both of them are given together with the LSV curves of bare GC and the LSV of our catalyst with iR drop correction for comparison purposes in Figure S3 (online SI section). From Figure S3, it is clear that none of them alone was able to deliver the potential that observed with DNA@IrO₂ NPs. This leads the conclusion that for an efficient electrocatalytic activity, the presence of both IrO₂ and DNA should be together and it is important too as we synthesized. The turn over frequency (TOF) of our catalyst was calculated as per previous studies on IrO₂.⁹³ The calculated TOF value is 7.88 s⁻¹ which is quite high and

comparable to the previous reports.⁹⁴ The detailed calculations regarding TOF values are given in online SI section. For comparison purposes, some of the important works with IrO₂ NPs were tabulated together in terms of their TOF values and given as Table 2. By analyzing Table 2, we found that the electrochemical water oxidation catalyzed by DNA@IrO₂ chain-like nano self-assemblies are one of the best reported for IrO₂ alone which required an overpotential of 312 mV to produce anodic current densities of 10 mA.cm⁻² with the TOF value of 7.88 s⁻¹. It is very clear when this value is compared with the bench marking study on OER by various metal oxide catalysts carried out by Jaramillo et al. which claimed that the current density of 10 mA.cm⁻² at 325 mV was the best ever efficiency for IrO₂ catalyst alone. However, it should not be forgotten that there are some important reports where IrO₂ was mixed with other metal oxides such as RuO₂⁹⁵ and Sb-SnO₂⁹⁶ for which the overpotential values were very close to the value we found from our study. Other than these, RuO₂ alone was also reported to be highly active in OER.⁹⁷ However, when one considers about the IrO₂ catalyst alone with the TOF value of 7.88 s⁻¹, our results is best one among the lowest few. The difference in the oxygen overpotential for OER between our catalyst and the report by Jaramillo et al. is found to be 13 mV which is significant in terms efficiency and this is mainly due to the synergism between the phosphate group on DNA that assisted the water coordination through its affinity toward water and the extreme electrocatalytic activity of IrO₂ towards OER. This is in good agreement with the earlier reports where they observed similar synergetic enhancement in OER.^{30,31,,50-54} The overall enhanced OER activity by our self-assembled DNA bound chain-like IrO₂ NPs is depicted schematically in Scheme 1. It is important to note that the synergism between the phosphate moiety of DNA and IrO₂ played a major role in the overall OER enhancement and in lowering the overpotential for the same. Finally, we conclude that the DNA@IrO₂ nano self-assemblies have shown the best efficiency ever reported for electrochemical water oxidation which gave 10 mA.cm⁻² of current density at 312 mV of oxygen overpotential which is the lowest oxygen overpotential ever reported for IrO₂ catalyst alone with the TOF value of 7.88 s⁻¹.

Conclusion

Self-assembled IrO₂ NPs had been synthesized for the first time by the room temperature reaction of IrCl₃ .xH₂O with NaBH₄ in the presence of DNA scaffold under continuous stirring within a short time. The chain-like morphologies of IrO₂ NPs were formed by tuning the concentration ratio of DNA and iridium salt solution. The potentiality of the IrO₂ NPs were

tested in two important applications, one as catalyst for the oxidation of 2-propanol to acetone where IrO₂ replaces the toxic dichromate reagent and other as an electrocatalyst for OER studies. From the catalysis study, it was observed that the reaction completed within 3 h time and the yield of the product and selectivity of the reaction is very high. Though the conductivity of DNA@IrO₂ NPs modified GC becomes comparatively lower than bare GC, the synergism assisted enhancement in the overall OER activity makes it worthier still. The OER study also revealed that the DNA@IrO₂ chain-like nano self-assemblies have been found to be one among the best for electrochemical water oxidation that requires a overpotential of 312 mV, to produce an anodic current densities of 10 mA cm⁻² with a significant TOF value of 7.88 s⁻¹ for IrO₂ catalyst alone. Synergism between the phosphate groups on DNA and the IrO₂ NPs towards OER gave combined and enhanced electrocatalytic activity that brings down the oxygen overpotential much lower compared to reported values with IrO₂ alone. Moreover, the present syntheses process is simple, less time consuming, reproducible and takes place at RT. Similarly, the present process can be extended further for the synthesis of other nanocatalyst for their specific applications in different interdisciplinary fields like organic catalysis, methanol and ethanol oxidation and ORR studies.

Supporting Information (SI) Available: The details about instrumental techniques, sample preparation for various characterizations and the determination of Turn Over Frequency (TOF) values are elaborated. Post cycle linear sweep voltammetry after chronoamperometry analysis and the control experiments on OER activities are also elaborated. The Figures related to EDS analysis, post cycle linear sweep voltammogram of GC electrode, control experiments are given as Figure S1, S2 and S3 respectively. The FT-IR bands of DNA experimentally observed in our study and the previously reported FT-IR bands were elaborated in Table S1. The formation of the self-assembled IrO₂NPs on DNA scaffold is depicted as Scheme S1. This material is available for free of charge via the Internet at <http://pubs.rsc.org>.

Acknowledgements: We wish to acknowledge Dr. Vijayamohanan K. Pillai, Director, and Dr. M. Jayachandran, HOD, ECMS division, CSIR-CECRI for their continuous support and encouragement. Authors also wish to acknowledge Dr. K. L. N. Phani, EEC division, and Dr. B.

Subramanian, ECMS division, CSIR-CECRI for their extended support during electrochemical studies. S. Anantharaj wishes to acknowledge council of scientific and industrial research (CSIR) for JRF fellowship. P. E. Karthik wishes to acknowledge university grant commission (UGC) for SRF fellowship. The support from the Central Instrumental Facility (CIF) and help from Mr. A. Rathishkumar (TEM in-charge, CIF) and Dr. S. Radhakrishnan (NMR in-charge) CSIR-CECRI, Karaikudi are greatly appreciated.

References.

- (1) S. Kundu and H. Liang, *Adv. Mater.*, 2008, **20**, 826.
- (2) S. Kundu, S. Lau and H. Liang, *J. Phys. Chem. C.*, 2009, **113**, 5150.
- (3) Y. N. Xia and N. J. Halas, *MRS Bull.* 2005, **30**, 338.
- (4) G. Kimuraa and K. Yamada, *Synth. Met.*, 2009, **159**, 914.
- (5) S. Kundu and U. Nithiyanantham, *Ind. Eng. Chem. Res.*, 2014, **53**, 13667.
- (6) U. Nithiyanantham, A. Ramadoss, S. R. Ede and S. Kundu, *Nanoscale.*, 2014, **6**, 8010.
- (7) S. Kundu, *J. Mater. Chem. C.*, 2013, **1**, 831.
- (8) L. E. Euliss, J. A. DuPont, S. Gratton, J. DeSimone, *Chem. Soc. Rev.*, 2006, **35**, 1095.
- (9) X. Chen, S. S. Mao, *Chem. Rev.*, 2007, **107**, 2891.
- (10) G. Liu and H. Zhang, *J. Phys. Chem. C.*, 2008, **112**, 2058.
- (11) Y. Gorlin and T. F. Jaramillo, *J. Am. Chem. Soc.*, 2010, **132**, 13612.
- (12) D. C. Papageorgopoulos, F. Liu and O. A. Conrad, *Electrochim. Acta.*, 2007, **53**, 1037.
- (13) J. Suntivich, H. A. Gasteiger, N. Yabuuchi and Y. Shao-Horn, *J. Electrochem. Soc.*, 2010, **157**, B1263.
- (14) Y. Lee, J. Suntivich, K. J. May, E. E. Perry and Y. Shao-Horn, *J. Phys. Chem. Lett.*, 2012, **3**, 399.
- (15) C. A. Mirkin, *Inorg. Chem.*, 2000, **39**, 2258.
- (16) L. Berti, A. Alessandrini and P. Facci, *J. Am. Chem. Soc.*, 2005, **127**, 11216.
- (17) C. F. Monson and A. T. Woolley, *Nano Lett.*, 2003, **3**, 359.
- (18) K. Keren, M. Krueger, R. Gilad, G. Ben-Yoseph, U. Sivan and E. Braun, *Science.*, 2002, **297**, 72.
- (19) U. Nithiyanantham, S. R. Ede and S. Kundu, *J. Mater. Chem. C.*, 2014, **2**, 3782.

- (20) R. Seidel, L. C. Ciacchi, M. Weigel, W. Pompe and M. Mertig, *J. Phys. Chem. B.*, 2004, **108**, 10801.
- (21) D. Sarker and M. Mandal, *J. Phys. Chem. C.*, 2012, **116**, 3227.
- (22) M. Hara and T. Mallouk, *Chem. Commun.*, 2000, 1903.
- (23) P. G. Hoertz, Y. I. Kim, W. J. Youngblood and T. Mallouk, *J. Phys. Chem. B.*, 2007, **111**, 6845.
- (24) T. Takagawa, C. A. Beasley and R. W. Murray, *J. Phys. Chem. C.*, 2009, **113**, 12958.
- (25) M. Yagi, E. Tomita and T. Kuwabara, *J. Electroanal. Chem.*, 2005, **579**, 83.
- (26) R.L. Doyle, I. J. Godwin, M. P. Brandon, M. E. G. Lyons, *Phys. Chem. Chem. Phys.* 2013, **15**, 13737.
- (27) P. Zhang, J. Zhang, J. Gong, *Chem. Soc. Rev.* 2014, **43**, 4271.
- (28) G. Li, H. Yu, X. Wang, S. Sun, Y. Li, B. Yi, Z. Shao, *Phys. Chem. Chem. Phys.* 2013, **15**, 2858.
- (29) W. J. Youngblood, S. A. Lee, Y. Kobayashi, E. A. Hernandez-pagan, P. G. Hoertz, T. A. Moore, A. L. Moore, D. Gust, T. E. Mallouk, *J. Am. Chem. Soc.* 2009, **131**, 926.
- (30) M. Sadakane, N. Rinn, S. Moroi, H. Kitatomi, T. Ozeki, M. Kurasawa, M. Itakura, S. Hayakawa, K. Kato, M. Miyamoto, S. Ogo, Y. Ide, T. Sano, *Z. Anorg. Allg. Chem.* 2011, **637**, 1467.
- (31) D. Liu, L. Jing, P. Luan, J. Tang, H. Fu, *ACS Appl. Mater. Interfaces* 2013, **5**, 4046.
- (32) M. Sadakane, E. Steckhan, *Chem. Rev.* 1998, **98**, 219.
- (33) A. Sartorel, M. Carraro, G. Scorrano, R. De Zorzi, S. Geremia, N. D. Mcdaniel, S. Bernhard, M. Bonchio, *J. Am. Chem. Soc.* 2008, **130**, 5006.
- (34) J. O. M. Bockris, T. Otagawa, *J. Electrochem. Soc.* 1984, **131**, 290.
- (35) R. Abe, M. Higashi, K. Domen, *J. Am. Chem. Soc.* 2010, **132**, 11828.
- (36) X. Zong, H. Yan, G. Wu, G. Ma, F. Wen, L. Wang, C. Li, *J. Am. Chem. Soc.* 2008, **130**, 7176.
- (37) A. A. Gambardella, S. W. Feldberg and R. Murray, *J. Am. Chem. Soc.*, 2012, **134**, 5774.
- (38) P. E. Karthik, K. A. Raja, S. Senthil Kumar, K. L. N. Phani, Y. Liu, S. -X. Guo, J. Zhang and A. Bond, *RSC Adv.*, 2015, **5**, 3196.
- (39) T. Reier, M. Oezaslan, P. Strasser, *ACS Catal.* 2012, **2**, 1766.
- (40) S. Kwon, F. -R. F. Fan, A. J. Bard, *J. Am. Chem. Soc.* 2010, **132**, 13165.

- (41) A. B. Dekanski, M. Mitric, V. V. Panic, S. K. Milonjic, V. B. Miskovic-Stankovic, B. Z. Nikolic, *Phys. Chem. Chem. Phys.* 2010, **12**, 7521.
- (42) T. Nakagawa, N. S. Bjorge, R. Murray, *J. Am. Chem. Soc.* 2009, **131**, 15578.
- (43) N. D. Morris, M. Suzuki, T. E. Mallouk, *J. Phys. Chem. A* 2004, **108**, 9115.
- (44) M. Yagi, E. Tomita, S. Sakita, T. Kuwabara, K. Nagai, *J. Phys. Chem. B Lett.* 2005, **109**, 21489.
- (45) W. Hu, Y. Wang, X. Hu, Y. Zhou, S. Chen, *J. Mater. Chem.* 2012, **22**, 6010.
- (46) H. N. Nong, L. Gan, E. Willinger, D. Teschner, P. Strasser, *Chem. Sci.* 2014, **5**, 2955.
- (47) Y. S. Nam, A. P. Magyar, D. Lee, J. Kim, D. S. Yun, H. Park, T. S. P. Jr, D. A. Weitz, A. M. Belcher, *Nat. Nanotechnol.* 2010, **5**, 340.
- (48) C. C. L. Mccrory, S. Jung, J. C. Peters, T. F. Jaramillo, *J. Am. Chem. Soc.* 2013, **135**, 16977.
- (49) K. A. Stoerzinger, L. Qiao, M. D. Biegalski, Y. Shao-horn, *J. Phys. Chem. Lett.* 2014, **5**, 1636.
- (50) M. W. Kanan, D. G. Nocera, *Science*, 2008, **321**, 1072.
- (51) S. -X. Guo, Y. Liu, A. M. Bond, J. Zhang, P. E. Karthik, I. Maheshwaran, S. Senthil Kumar, K. L. N. Phani, *Phys. Chem. Chem. Phys.*, 2014, **16**, 19035.
- (52) L. -A. Stern, L. Feng, F. Song, X. Hu, *Energy Environ. Sci.*, 2015, **8**, 2347.
- (53) L. Li, S. -H. Chai, S. Dai, A. Manthiram, *Energy Environ. Sci.*, 2014, **7**, 2630.
- (54) L. Li, A. Manthiram, *J. Mater. Chem. A*, 2013, **1**, 5121.
- (55) B. R. Travis, R. S. Narayan, B. Borhan, *J. Am. Chem. Soc.* 2002, **124**, 3824.
- (56) G. Y. Li, *Angew. Chem.* 2001, **113**, 1561.
- (57) L. Yin, J. Liebscher, *Chem. Rev.* 2007, **107**, 133.
- (58) T. Katsuki, K. B. Sharpless. *J. Am. Chem. Soc.* 1980, **102**, 5974.
- (59) T. Punniyamurthy, S. Velusamy, J. Iqbal, *Chem. Rev.* 2005, **105**, 2329.
- (60) A. Gervasini, *Catal. Lett.* 1997, **43**, 219.
- (61) Y. Zhao, E. A. Hernandez-Pagan, N. M. Vargas-Barbosa, J. L. Dysart and T. E. Mallouk, *J. Phys. Chem. Lett.*, 2011, **2**, 402.
- (62) G. S. Nahor, P. Hapiot, P. Neta and A. Harriman, *J. Phys. Chem.*, 1991, **95**, 616.
- (63) J. R. Jensen, M. L. Duval, K. L. Kelly, A. A. Lazarides, G. C. Shatz and R. P. Van, Duyne, *J. Phys. Chem. B.*, 1999, **103**, 9846.
- (64) A. Harriman, J. M. Thomas and G. R. Millward, *New J. Chem.*, 1987, **11**, 757.

- (65) R. –S. Chen, Y. –S. Huang, Y. –M. Liang, D. –S. Tsai, Y. Chic and J. Kaid, *J. Mater. Chem.*, 2003, **13**, 2525.
- (66) Y. –M. Chang, Y. –C. Hsieh, P. –W. Wu, C. –H. Lai and T. –Y. Chang, *Mater. Lett.*, 2008, **62**, 4220.
- (67) M. M. Can, S. I. Shah, M. F. Doty, C. R. Haughn, T. Firat, *J. Phys. D: Appl. Phys.* 2012, **45**, 195104.
- (68) R. Nyholm, A. Berndtsson, N. Mårtensson, *J. Phys. C: Solid St. Phys.* 1980, **13**, L1091.
- (69) C. A. Strydom, H. J. Strydom, *Inorganica Chimica Acta* 1989, **159**, 191.
- (70) D.R. Dreyer, S. Park, C. W. Bielawski, R. S. Ruoff, *Chem. Soc. Rev.* 2010, **39**, 228.
- (71) B. Basly, G. Popa, S. Fleutot, B. P. Pichon, A. Garofalo, C. Ghobril, C. Billotey, A. Berniard, P. Bonazza, H. Martinez, D. Felder-Flesch, S. Begin-Colin, *Dalton Trans.* 2013, **42**, 2146.
- (72) M. Rubel, R. Haasch, P. Mrozek, A. Wieckowski, C. De. Pauli, S. Trassati, *Vacuum* 1994, **45**, 423.
- (73) E. K. Galanos, D. E. Petrakis, V. N. Stathopoulos, P. J. Pomonis, D. P. Labou, A. T. Sdoukos, *Phys. Chem. Chem. Phys.* 2002, **4**, 3894.
- (74) K. Kudo, D. Mitsuoka, M. Takasuga, Y. Sugiyama, K. Sugawara, N. Katayama, H. Sawa, H. S. Kubo, K. Takamori, M. Ichioka, T. Fujii, T. Mizokawa, M. Nohara, *Sci. Rep.* 2013, **3**, 3101.
- (75) S. –J. Choi, W. –H. Ryu, S. –J. Kim, H. –J. Cho, I. –D. Kim, *J. Mater. Chem. B* 2014, **2**, 7160.
- (76) A. K. Shukla, A. M. Kannan, M. S. Hegde, J. Gopalakrishnan, *Journal of Power Sources* 1991, **35**, 163.
- (77) B. Kumar, M. Asadi, D. Pisasale, S. Sinha-Ray, B. A. Rosen, R. Haasch, J. Abiade, A. L. Yarin, A. Salehi-Khojin, *Nat. Commun.* 2013, **4**, 2819.
- (78) J. Shalini, K. J. Sankaran, C. –L. Dong, C. –Y. Lee, N. –H. Tai, I-N. Lin, *Nanoscale* 2013, **5**, 1159.
- (79) X. Zhong, J. Jin, S. Li, Z. Niu, W. Hu, R. Li, J. Ma, *Chem. Commun.* 2010, **46**, 7340.
- (80) S. Cobo, J. Heidkamp, P. –A. Jacques, J. Fize, L. Guetaz, B. Jousseleme, V. Ivanova, H. Dau, S. Palacin, M. Fontecave, V. Artero, *Nat. Mater.* 2012, **11**, 802.
- (81) M. Peuckert, *Electrochimica Acta* 1984, **29**, 1315.

- (82) G. Deniau, L. Azoulay, P. Jégou, G. L. Chevallier, S. Palacin, *Surface Science* 2006, **600**, 675.
- (83) L. Li, Y. Pan, L. Chen, G. Li, *Solid State Chem.* 2007, **180**, 2896.
- (84) M. Banyay, M. Sarkar, A. A. Graslund, *Biophys. Chem.* 2003, **104**, 477.
- (85) W. R. Mason III, H. B. Gray, *Inorg. Chem.* 1968, **7**, 55.
- (86) S. L. Suib, A. Kostapapas, D. Psaras, *J. Am. Chem. Soc.* 1984, **106**, 1614.
- (87) S. Hussain, T. Surendra, M. Farooqui, *J. Chem. Pharm. Res.* 2012, **4**, 4406.
- (88) J. W. Nicoletti, G. M. Whitesides, *J. Phys. Chem.* 1989, **93**, 759.
- (89) C. A. C. Sequeira, D. M. F. Santos, P. S. D. Brito, *Appl. Surf. Sci.* 2006, **252**, 6093.
- (90) M. Stern, A. L. Geary, *J. Electrochem. Soc.* 1957, **104**, 56.
- (91) A. J. Bard, L. R. Faulkner, *Electrochemical Methods Fundamentals and Applications*, Wiley, New York, 2nd edn., 2001 (Pages 100-106).
- (92) T. Shinagawa, A. T. Garcia-Esparza, K. Takanabe, *Sci. Reports.* 2015, **5**, 131801.
- (93) S. Wehner, J. Cisternas, O. Descalzi, J. Küppers, *Eur. Phys. J. Special Topics* 2014, **223**, 21.
- (94) M.-C. Chuang, J.-A. A. Ho, *RSC Adv.* 2012, **2**, 4092.
- (95) L. -E. Owe, M. Tsytkin, K. S. Wallwork, R. G. Haverkamp, S. Sunde, *Electrochim. Acta*, 2012, **70**, 158.
- (96) A. Marshall, R. Haverkamp, *J. Mater. Sci.* 2012, **47**, 1135.
- (97) H. C. Ma, C. P. Liu, J. H. Liao, Y. Su, X. Z. Xue, W. Xing, *Journal of Molecular Catalysis A: Chemical* 2006, **247**, 7.

Figure Captions:

Figure 1: UV-Visible (UV-Vis) absorption spectra of the different solution mixture used for the formation IrO₂ NPs on DNA. (A) Curve a is the absorption spectrum of IrCl₃ · xH₂O salt solution; curve b is the absorption band of aqueous DNA solution; curve c shows the absorption band of the mixture of iridium chloride salt solution with DNA; curve d and e shows the absorption band of chain-like IrO₂ NPs with smaller and larger sizes of the individual particles at different DNA concentration. (B) is the enlarged absorption band of the IrO₂ NP for two different sets as indicated a, and b respectively. The inset of Figure (A) shows the synthesized DNA@IrO₂ solutions with two different color.

Figure 2: Transmission Electron Microscopy (TEM) image of the DNA@IrO₂ NPs. Figure 2, A-C are the low and high magnified TEM images of DNA@IrO₂ NPs having smaller average particle size and Figure 2D and 2E are the HR-TEM micrograph and corresponding SAED patterns. Figure 2, F-H is the TEM micrographs of the IrO₂ NPs having larger average particle size and Figure 2I and 2J are the HR-TEM micrograph and corresponding SAED patterns. The inset of Figure 2C and Figure 2H shows corresponding particle size distribution histograms.

Figure 3: X-ray diffraction (XRD) pattern of the DNA@IrO₂ in the 2 θ range of 10-90°. Curve a and b shows the XRD pattern for two different morphology of IrO₂.

Figure 4: X-ray photoelectron spectroscopic (XPS) analysis of DNA@IrO₂ NPs where (A) is the survey spectrum; (B) is the high resolution scan for Ir 4d; (C) is the high resolution scan for Ir 4f, (D) is the high resolution scan for C 1s, (E) is the high resolution scan for P 2p and (F) is the high resolution scan for O 1s and (G) is high resolution scan for N 1s respectively.

Figure 5: The Fourier-transform infrared (FT-IR) spectra of bare DNA (curve a) and DNA@IrO₂ NPs (curve b) in the wavenumber range 400-4000 cm⁻¹.

Figure 6: (A) UV-Visible absorption spectra for the catalysis reaction. Curve a is for only 2-propanol; curves b and c correspond to the absorption spectrum of the reaction mixture of 2-propanol, sulphuric acid and IrO₂ catalyst before and after reaction and curve d is the absorption spectrum of the product acetone. (B) FT-IR spectrum of 2-propanol (a) and FT-IR spectrum of the product acetone (b). (C) FT-NMR spectra of the reactant 2-propanol (curve a) and the product acetone (curve b).

Figure 7: (A) Linear sweep voltammograms (LSV) of electrochemical water oxidation by DNA bound IrO₂ chain-like nano self-assemblies. Line a is the LSV of the same electrochemical water oxidation by DNA@IrO₂ chain-like nano self-assemblies with iR drop correction. Line b is the LSV of the same electrochemical water oxidation by DNA bound IrO₂ chain-like nano self-assemblies without iR drop correction. (B) Electro Impedance Spectrum (EIS) of the same DNA@IrO₂ modified GC electrode. (C) Electro Impedance Spectrum (EIS) of the same DNA modified GC electrode. (D) Electro Impedance Spectrum (EIS) of the same IrO₂ modified GC electrode.

Figure 8: (A) Steady state polarization curve of the electrochemical water oxidation by DNA@IrO₂ chain-like nano self-assemblies. (B) The current Vs time profile of the chronoamperometric study carried out using DNA@IrO₂ chain-like nano self-assemblies.

Figure 9: CV (iR free) at 10 mV/s for DNA@IrO₂ NPs modified GC is given upto 200th cycle (indicated with different color).

Table 1: Summary of detailed final concentrations of all the reaction parameters, time of reaction, particles size, shape etc.

Table 2: Comparison of catalytic efficiency with our catalyst and the corresponding TOF values of earlier reports are highlighted.

Scheme 1: Schematic depiction for the overall OER process with DNA@IrO₂ nano self-assemblies.

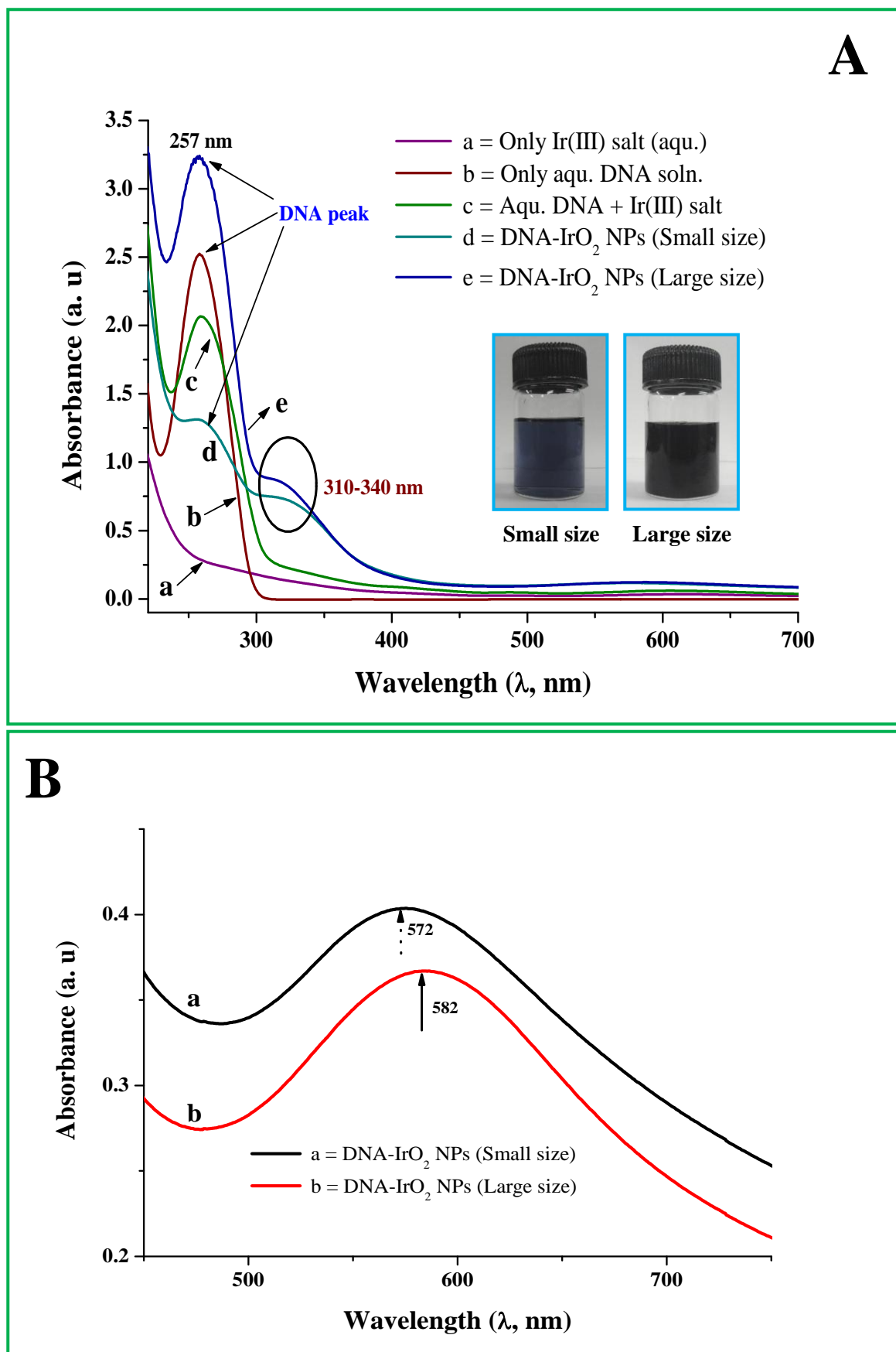


Figure 1, A-B

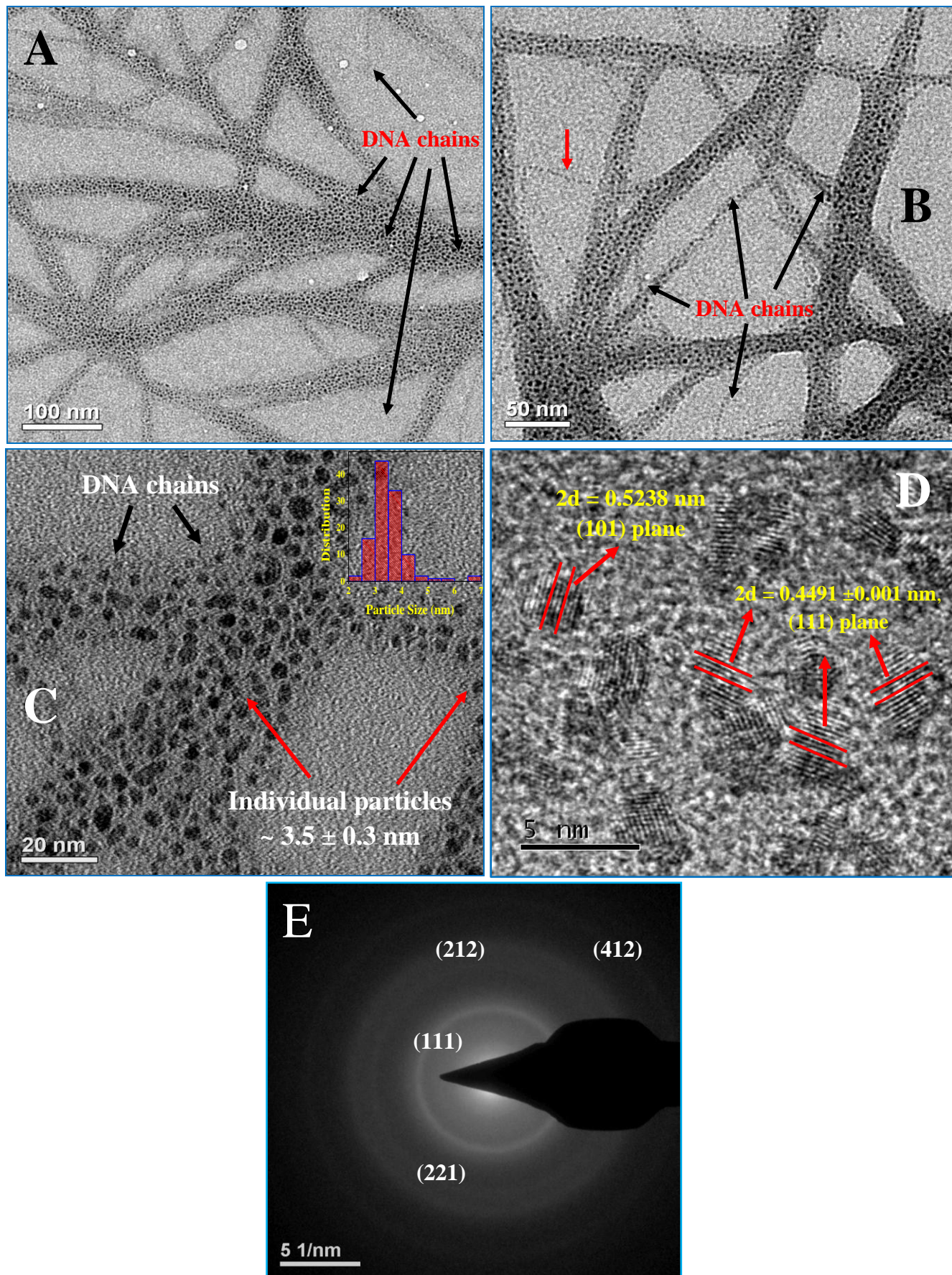


Figure 2, A-E

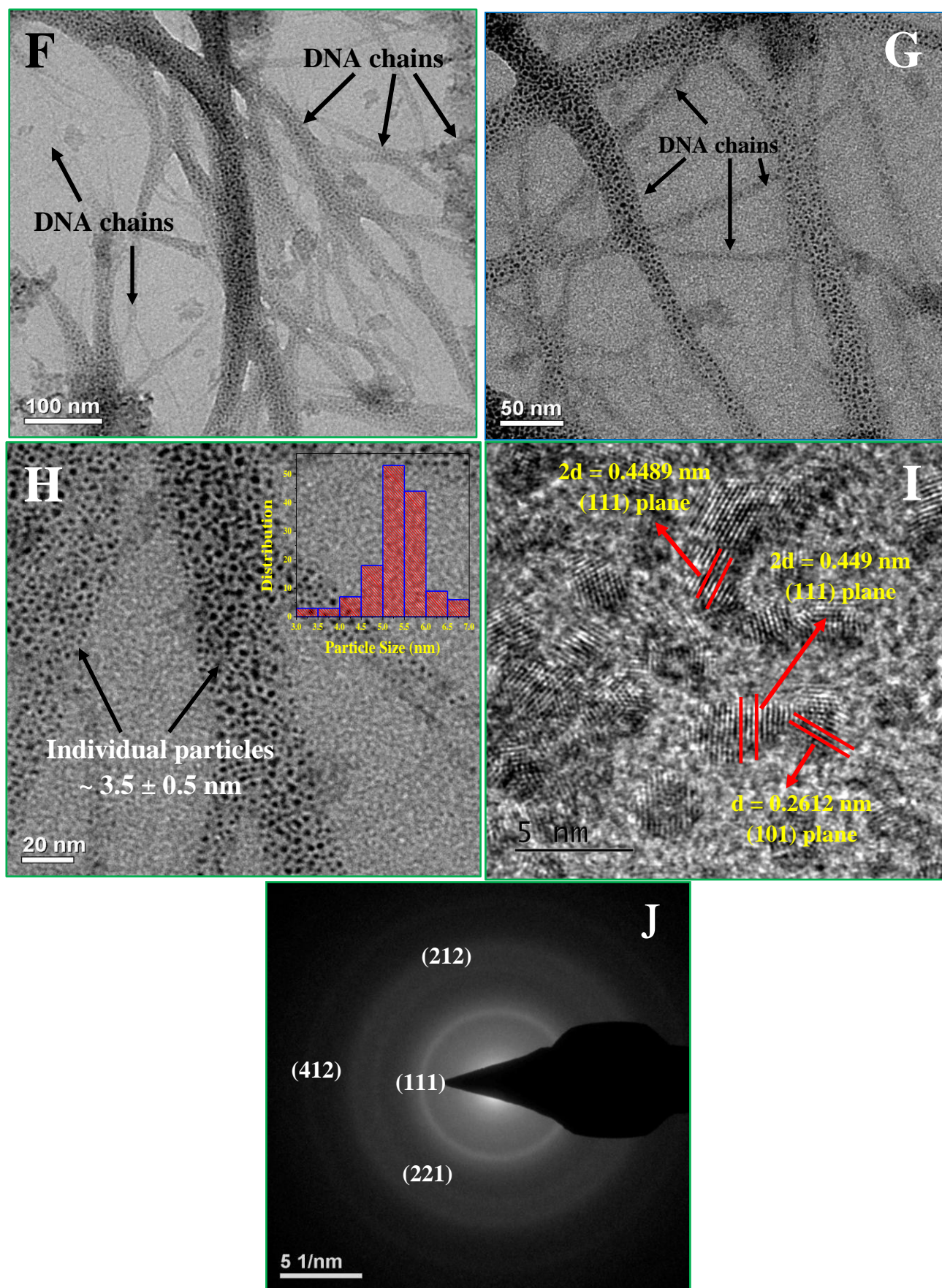


Figure 2, F-J

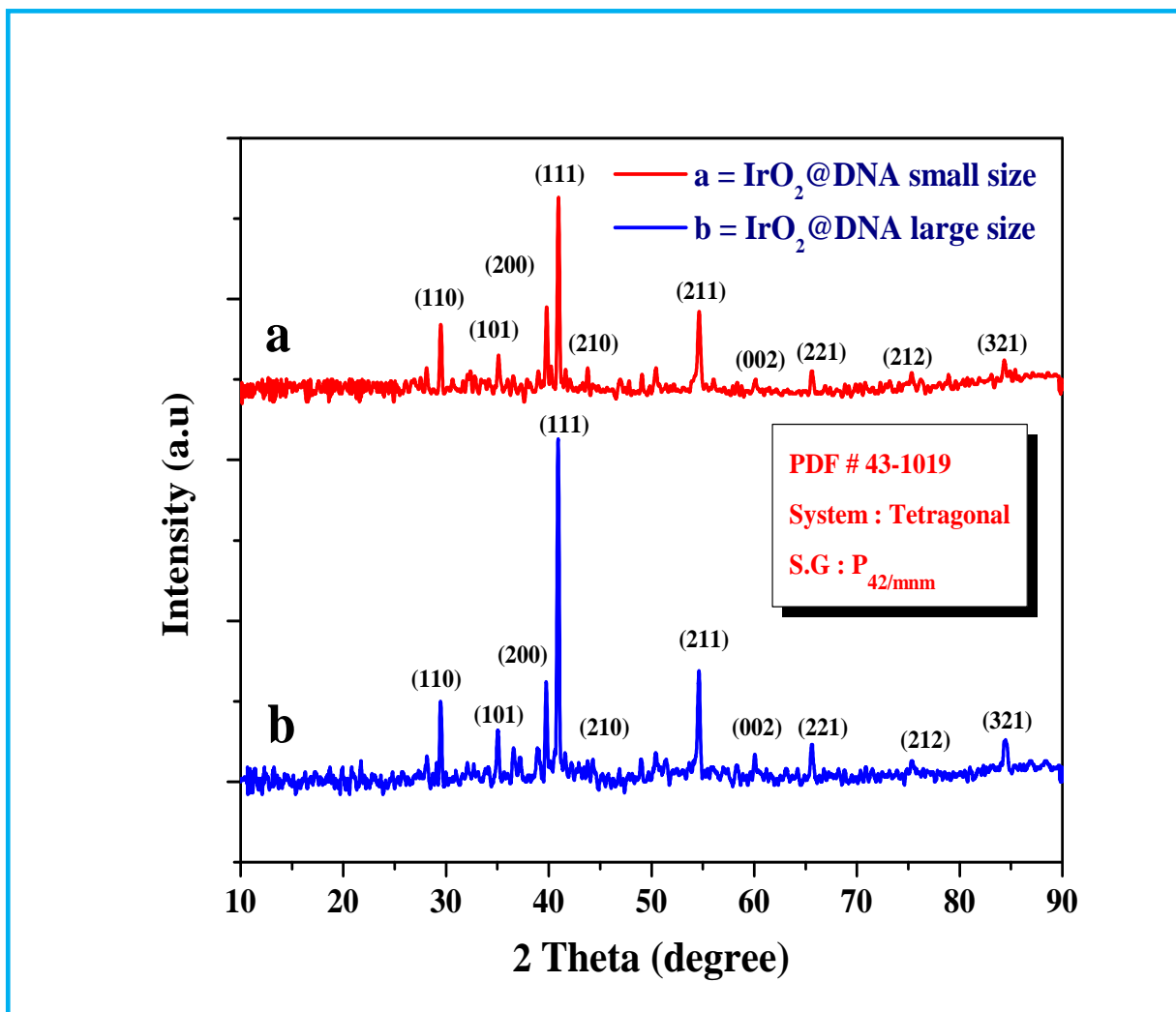


Figure 3

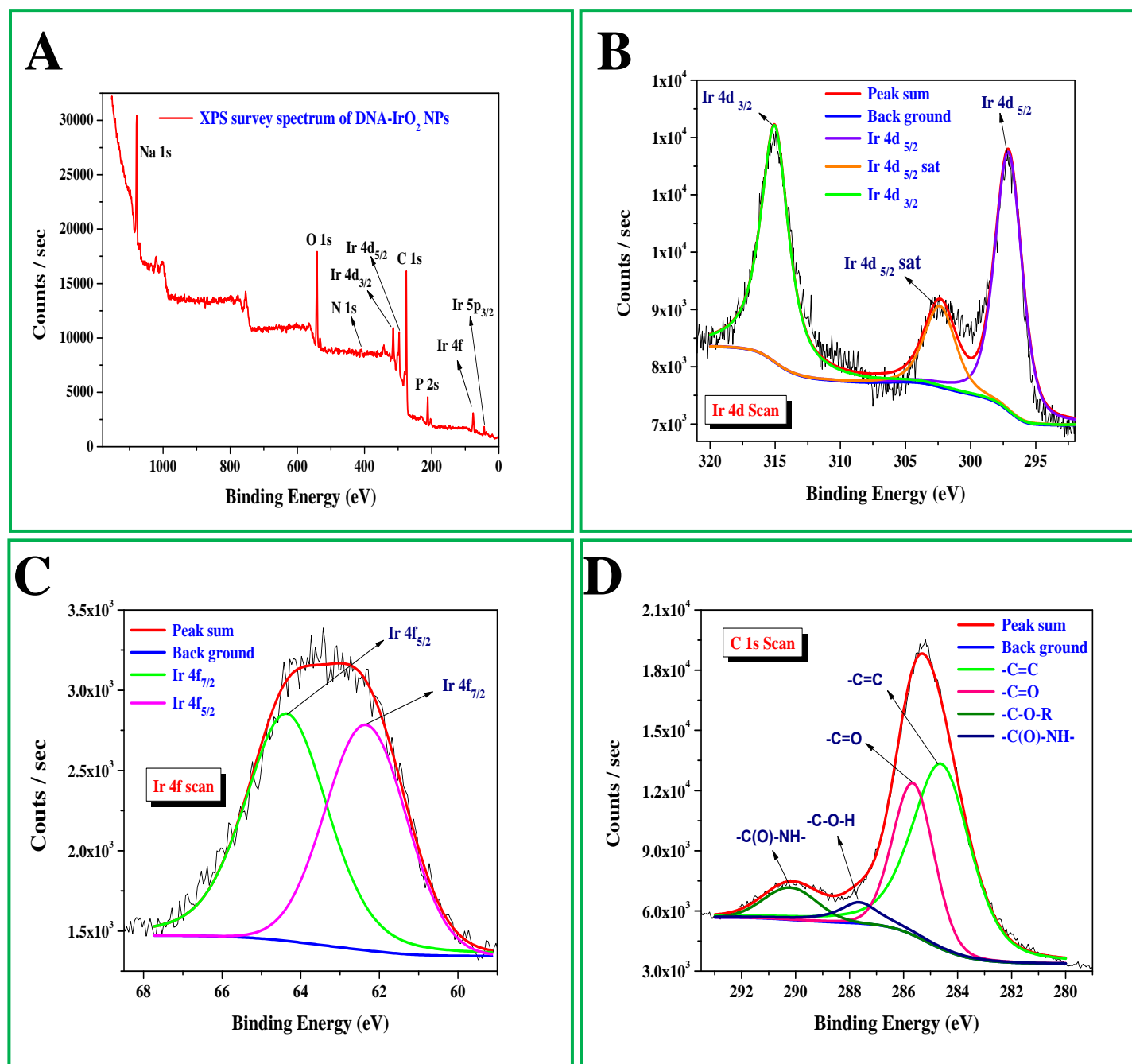
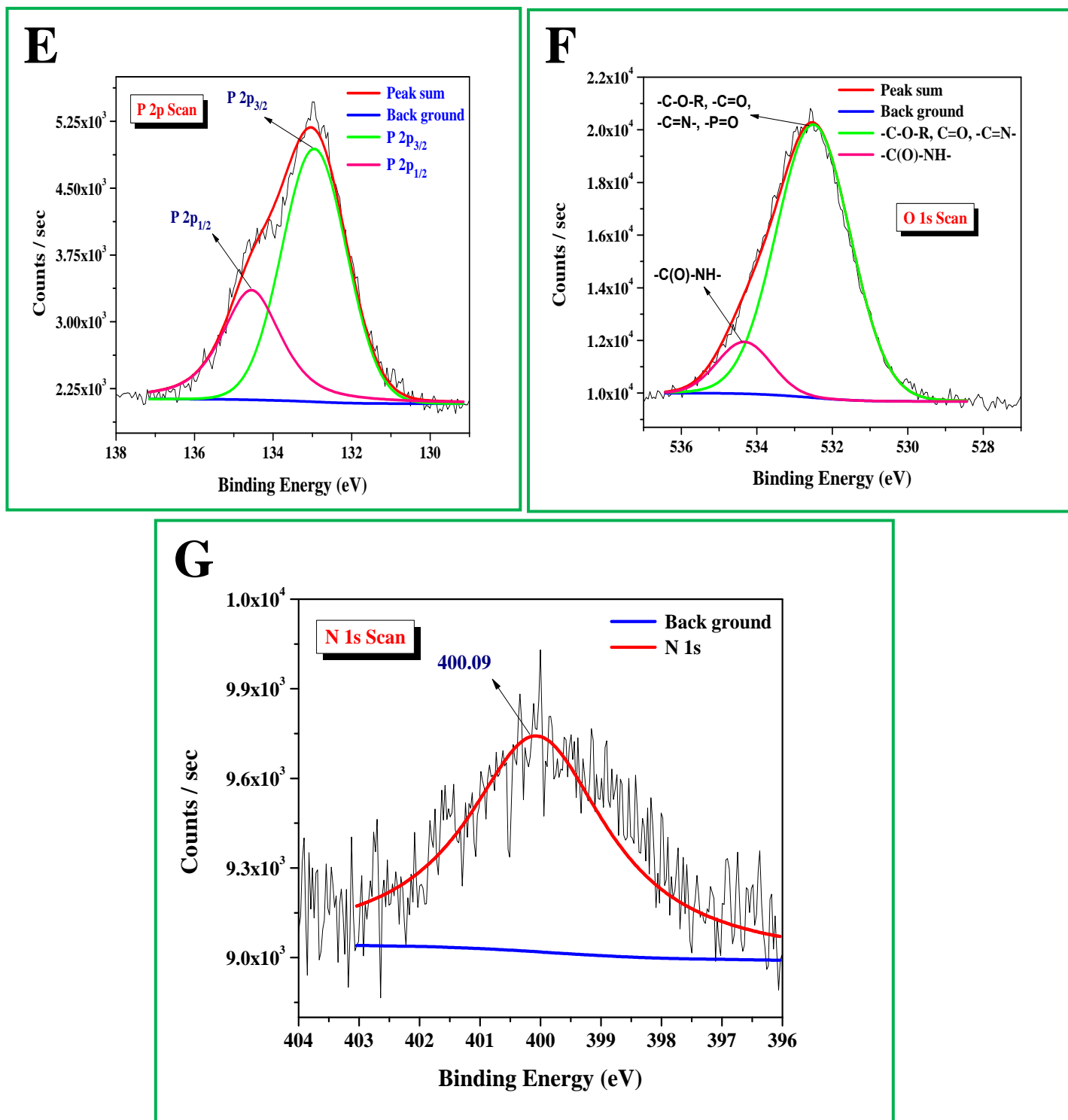


Figure 4, A-D



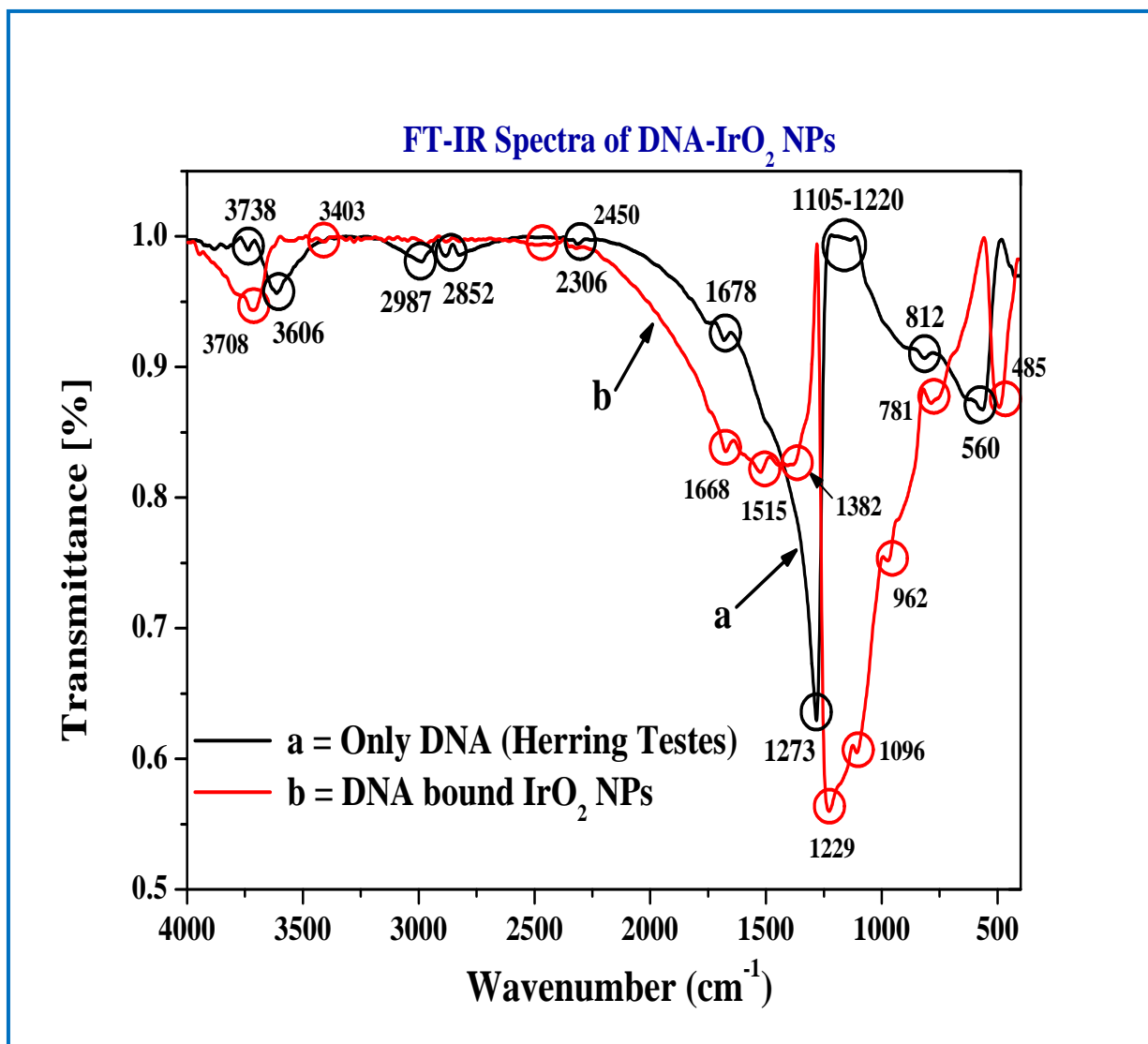


Figure 5

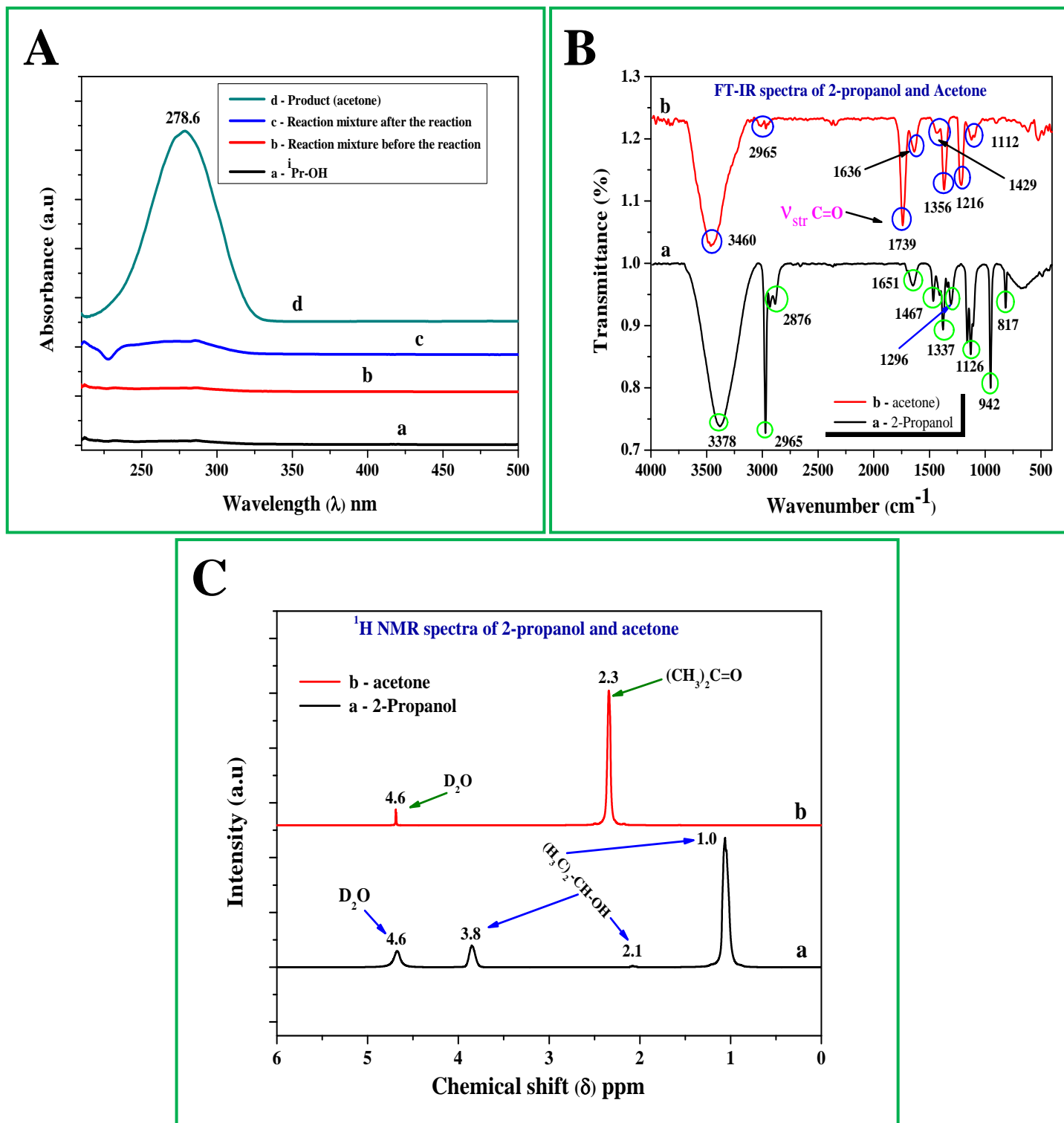


Figure 6, A-C

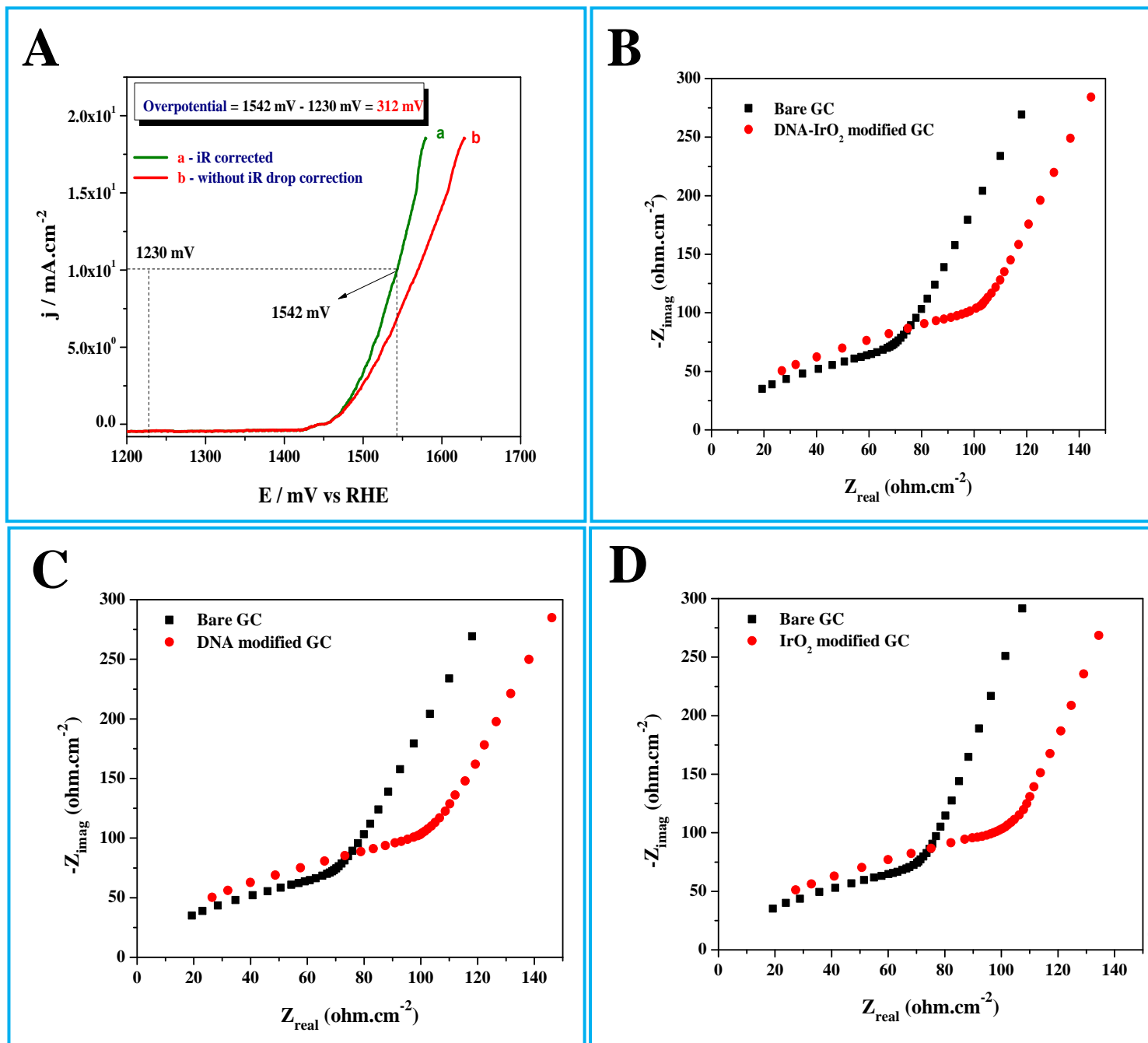


Figure 7, A-D

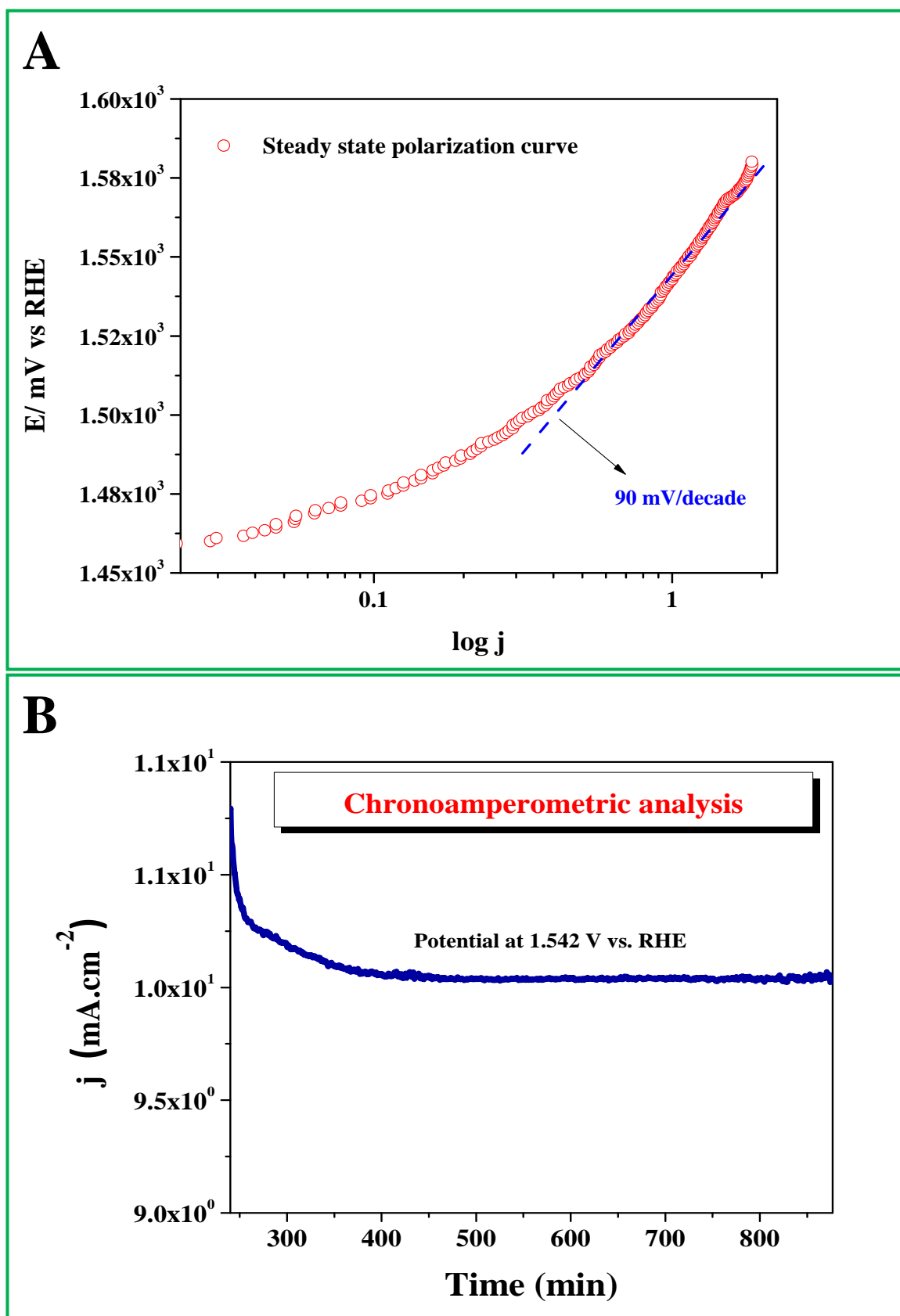


Figure 8, A-B

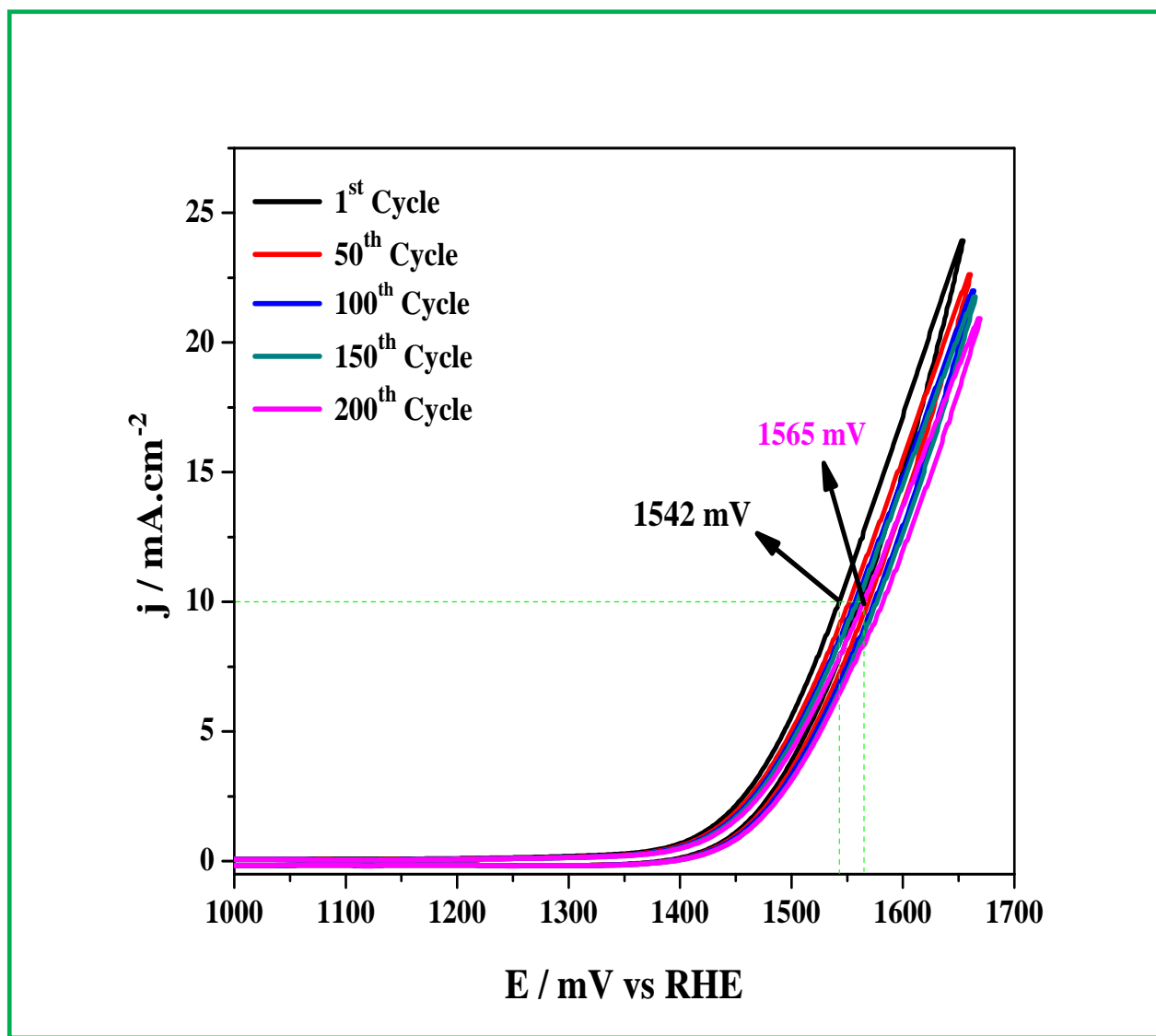


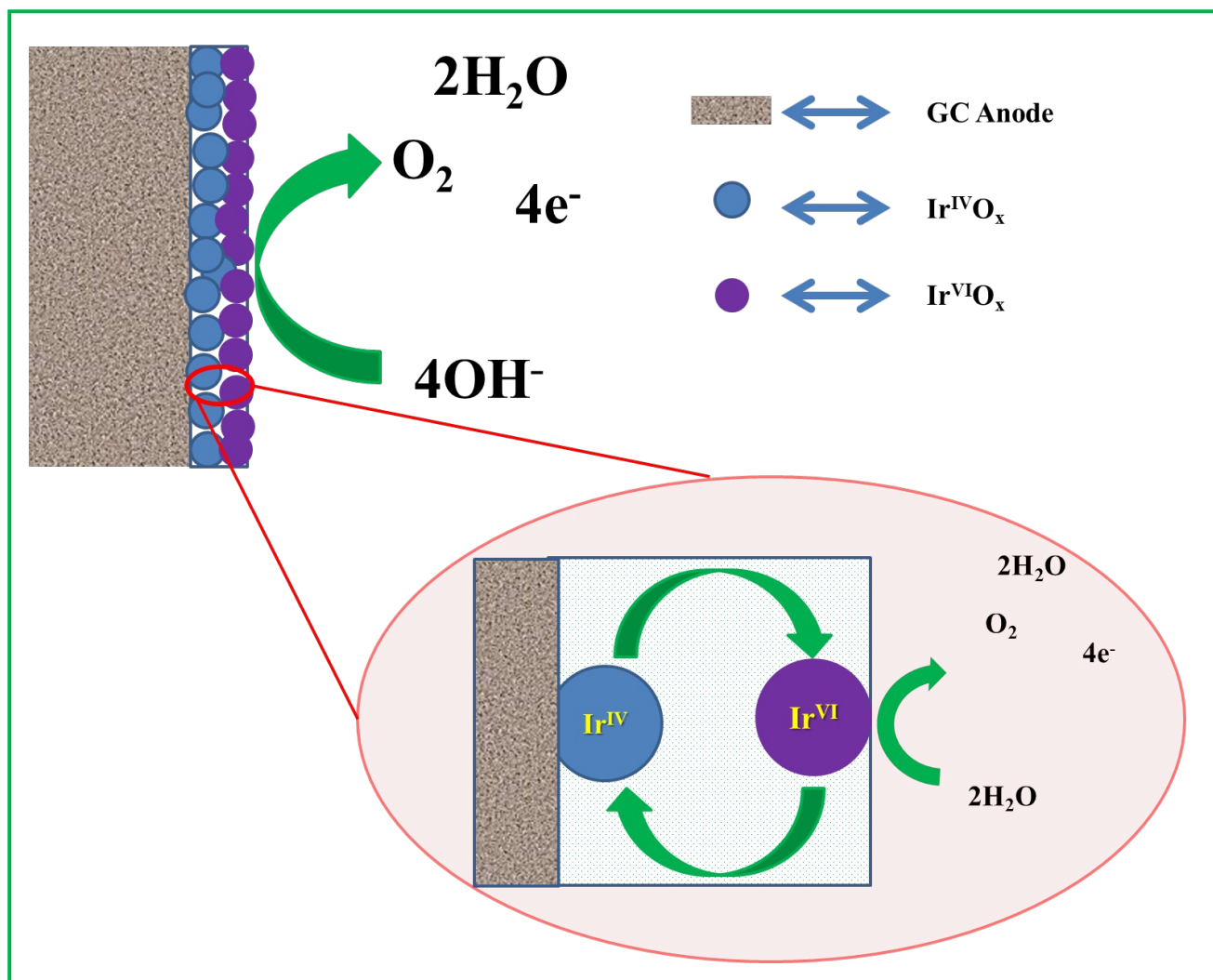
Figure 9

Table 1

Set no.	Final conc. of DNA (M)	Final conc. of IrCl ₃ .H ₂ O (M)	Conc. of NaBH ₄ added (M)	Total volume of the reaction mixture (mL)	Total reaction time (min)	Color of the DNA@IrO ₂ soln. with λ_{\max} values (nm)	Shape and dimension of the particles (nm)
1	1.00×10^{-2}	1.66×10^{-4}	0.1	12	5	Light bluish, Broad band 310-340 and 572	Self-assembled, chain-like, $\sim 3.5 \pm 0.3$ nm
2	7.05×10^{-2}	1.66×10^{-4}	0.1	12	45	Dark bluish, Broad band 310-340 and 582	Self-assembled, chain-like, $\sim 5.5 \pm 0.3$ nm

Table 2

Benchmarking the DNA@IrO₂ NPs (present work) against other IrO_x electrocatalysts			
S. No	Preparation method of the catalyst	TOF value	Reference No.
1	Via the SAM interaction of ITO and IrO _x colloids	6.66	80
2	Through polyallylamine assisted deposition of IrO ₂ on GC electrode	6.36	89
3	Anodic deposition from homogeneous medium	8-11	78
4	Electroless deposition of IrO _x on anodized Au surface	6.30	23
5	By Electroflocculation	6.6	24
6	DNA@IrO₂ NPs on GC electrode	7.88	Present work



Scheme 1

Table of Contents

Self-assembled IrO₂ Nanoparticles on DNA Scaffold with Enhanced Catalytic and Oxygen Evolution Reaction (OER) Activities



Text

Self-assembled IrO₂ nanoparticles on DNA scaffold exhibit an excellent material for organic catalysis reaction and as an excellent electrocatalyst for oxygen evolution reaction (OER) studies.
